6-14-2012

Application of an Imaging Fourier-Transform Spectrometer for the Means of Combustion Diagnostics

Michael R. Rhoby

Follow this and additional works at: https://scholar.afit.edu/etd

Part of the Optics Commons

APPLICATION OF AN IMAGING FOURIER-TRANSFORM SPECTROMETER FOR THE MEANS OF COMBUSTION DIAGNOSTICS

THESIS

Michael R. Rhoby, Civilian

AFIT/OSE/ENP/12-J02

DEPARTMENT OF THE AIR FORCE
AIR UNIVERSITY

AIR FORCE INSTITUTE OF TECHNOLOGY

Wright-Patterson Air Force Base, Ohio

The views expressed in this document are those of the author and do not reflect the official policy or position of the United States Air Force, the United States Department of Defense or the United States Government. This material is declared a work of the U.S. Government and is not subject to copyright protection in the United States.

AFIT/OSE/ENP/12-J02

APPLICATION OF AN IMAGING FOURIER-TRANSFORM SPECTROMETER

FOR THE MEANS OF COMBUSTION DIAGNOSTICS

THESIS

Presented to the Faculty

Department of Engineering Physics

Graduate School of Engineering and Management

Air Force Institute of Technology

Air University

Air Education and Training Command

in Partial Fulfillment of the Requirements for the

Degree of Master of Science in Optical Sciences and Engineering

Michael R. Rhoby, B.S.

Civilian

June 2012
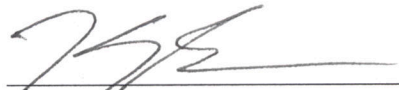
AFIT/OSE/ENP/12-J02

APPLICATION OF AN IMAGING FOURIER-TRANSFORM SPECTROMETER

FOR THE MEANS OF COMBUSTION DIAGNOSTICS

Michael R. Rhoby, B.S.

Approved:

_____

Kevin C. Gross, PhD (Chairman)

8-Jun-2012

Date

_____

Glen P. Perram, PhD (Member)

8 Jun 2012

Date

_____

Marc D. Polanka, PhD (Member)

5 JUNE 2012

Date

Abstract

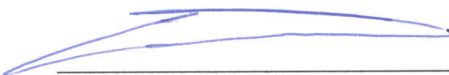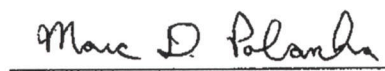A passive remote sensing technique for accurately monitoring the combustion efficiency of petrochemical flares is greatly desired. A Phase II DOE-funded SBIR lead by Spectral Sciences, Inc. is underway to develop such a method. This paper presents an overview of the current progress of the Air Force Institute of Technology's contribution to this effort. A Telops Hyper-Cam Mid-wave infrared (MWIR 1800–6667 cm^{-1} or 1.5–5.5 μm) imaging Fourier-transform spectrometer is used to examine a laminar calibration flame produced by a Hencken burner. Ethylene fuel (C_2H_4) was burned at four different equivalency ratios $\Phi = 0.80, 0.91, 1.0$ and 1.25. Presented is qualitative spectrally-resolved visualization of a Hencken burner flame and the spatial distribution of combustion by-products. The flame spectra were characterized by structured emissions from CO_2, H_2O and CO. Measurements of scalar values are also critical for validating chemical kinetic models, understanding new combustion phenomenon, and verifying numerical simulations. A single-layer model is developed to estimate the temperature and H_2O and CO_2 concentrations at varying heights above the burner using spectrally-resolved flame emissions between 3100 $cm^{-1} \leq \nu \leq 3500$ cm^{-1} (2.86 μm $\leq \lambda \leq 3.23$ μm). At the flame center 10 mm above the burner, temperature was estimated as T = 2172 ± 28 K, and this compares favorably with both recently reported OH-absorption measurements (T = 2226 ± 112 K) and equilibrium calculations (T = 2302 K). H_2O and CO_2 mole fractions across the flame at the same height of 10 mm were measured to be 13.7 ± 0.6% and 15.5 ± 0.8%, respectively. Advantages and limitations of this new technique are discussed.

Acknowledgements

Foremost, I would like to express my sincere gratitude to my advisor Dr. Kevin Gross for the continuous support of my study and research, for his patience, motivation, enthusiasm, and knowledge. His guidance helped me in all areas of research and writing, I could not have completing this work without him.

I would also like to thank my family and friends for their patience and continued support. First my fiancée for her nightly encouragement and motivation. It was her kind words that continually centered my determination. Also I credit Jacob as he was always available for relevant discussions and editing advice and at the very least stress reducing comic relief. Finally I credit Capt Harley for his mentoring role throughout this entire experience. His previous knowledge saved me countless hours.

Michael R. Rhoby

Table of Contents

List of Figures

Figure		Page

x

List of Tables

List of Abbreviations

APPLICATION OF AN IMAGING FOURIER-TRANSFORM SPECTROMETER FOR THE MEANS OF COMBUSTION DIAGNOSTICS

I. Introduction

When combustion from sources such as industrial flares is inefficient, soot and Highly-Reactive Volatile Organic Compounds (HR-VOCs) form and are released into the atmosphere posing environmental and health risks. Flares can sustain levels of Combustion Efficiency[1] (CE) greater than 95% [1, 2, 3], however even a small drop in CE can represent a large release of HR-VOCs into the atmosphere. This has made the creation of a fast, accurate, standoff method of CE monitoring an industry priority. Several accepted CE measurement techniques are in use today and are discussed in Chapter II of this work. However, prevalent issues faced by these techniques have lead to the proposal of a new alternative method utilizing Imaging Fourier Transform Spectroscopy (IFTS). Spectral Sciences is leading a project in conjunction with The University of Utah and The Air Force Institute of Technology (AFIT) to develop a system for the real-time remote monitoring of CE and HR-VOCs in industrial flares. The University of Utah team will apply their state-of-the-art Computational Fluid Dynamic (CFD) and chemical reaction models to predict flare flow-field parameters including temperature, gas density, and species concentrations throughout the entire flare plume. Spectral Sciences are developing the radiative transfer models necessary to simulate flare plume spectra in the infrared. AFIT is standing up a laboratory scale flare testing facility and will provide temporally and spatially resolved infrared spectra which will be used to validate and improve the

---

[1] Combustion efficiency is defined as the ratio of carbon converted to CO_2 relative to the total amount of carbon in the fuel.

reactive-flow CFD and radiative transfer models. Although the ultimate goal is an accurate measurement of the CE of an industrial flare, this document focuses on the initial work required to validate the use of an IFTS camera as a tool for Combustion Diagnostics (CD) for open burning flames.

1.1 Research approach

As described above, the focus of this work is to establish IFTS as a valid tool for use in combustion diagnostics. Achieving this requires both a qualitative and quantitative understanding of a flame source accepted in the CD community with the quantitative results matching well with previous work. This work then started with an interrogation of a laminar flame burning several fuel to air ratios, emphasizing the qualitative investigation of the flame's structure and a development of a basic understanding of the flame spectrum. Although the qualitative investigation is not groundbreaking, it does provide information such as dimensions, chemical composition and rough chemical distribution useful in adapting a single layer radiative transfer model for concentration estimation already established [4, 5]. This adaption of the model and its initial results are the focus of the second half of this work. The results of temperature and mole-fraction calculations are in good agreement with values estimated in a previous work [6]. The developed model is currently simple, assuming a single layer through the flame. A more sophisticated model is necessary for more accurate results and is under development for future work

1.2 Document structure

Chapter II provides a synopsis of the most relevant techniques and articles referenced in this work. Included is an overview of some current methods used in CD, a short review of previous IFTS work, and an introduction to laminar flames. Chapters

III and IV present two articles on the topic of mid-wave IFTS measurements of laboratory scale laminar flames. Chapter III was accepted for oral presentation at the SPIE Defense, Security, and Sensing 2012 conference. This paper focuses primarily on the qualitative visualization of the flame, providing imagery and spectral comparisons of several laminar flames. The second paper, Chapter IV, was accepted for oral presentation at the Spring Technical Meeting of the Central States Section of the Combustion Institute 2012. It focuses on the development of a single layer spectral model capable evaluating two-dimensional scalar values such as temperature and mole fraction. There is some overlap in content between these two papers and Chapters I and II of this document. Despite this the conference papers are presented in their entirety. Chapter V summerises the overarching conclusions and main takeaways of this work. Appendix A presents an early work accepted for oral presentation at the SPIE Optics + Photonics 2011 conference. This work also presents a qualitative investigation into laminar flames utilizing a long-wave IFTS camera, rather than mid-wave, and two different fuel types. It has been left as an appendix however because low levels of spectrally diverse chemical signal in the long-wave has currently proven less insightful than that of the mid-wave. Appendix B provides an expanded discussion of a model in Chapter III used to understand the effects a harmonic pulsation in the flame has on the spectral line-shape. Appendix C provides additional discussion on the calibration if the IFTS camera performed in Chapters 3 and 4. Appendix D provides a detailed breakdown of the components of the spectral radiance model used in Chapters 3 an 4.

II. Background

Monitoring of combustion efficiency is a well established field with a host of detection techniques, each aiming to maximize the combination of three goals: high simultanious species resolution, low concentration detection and spatial resolution. A select few of these techniques, divided into the two major categories of active and passive sensing, are discussed in this section. These methods were chosen because they show some of the most common trade-offs between the three goals. This review will lead itself into a discussion of the proposed IFTS alternative; including previous work showing the capabilities of IFTS as a combustion diagnostics tool. Following this will be a review regarding laminar flames and an experiment performed by Meyer et. al.[6]

2.1 Active Diagnostic Sensing Techniques

Probe sampling is a strait forward method used for continuous monitoring of waste gasses from combustion sources. Built in *in situ* equipment is ideal for this type of monitoring, however many combustion sources in use are not equipped with these probes. External point sampling, or placing a temporary probe in the combustion exhaust, has been utilized but can be less than practical due to the equipment required to keep the probe in position [7]. In situations such as the study done by McDaniel on the combustion efficiency of industrial flares, the sampling point can be high off the ground requiring a crane or other large equipment [7]. Such large equipment is cumbersome and hard to adjust if changing winds move the desired sampling point. Probing also fails to provide spacially resolved information in a single aquisition. The dynamic nature of combustion and the entrainment of ambient gasses generally leads to a diverse distribution of temperature and chemical concentrations. An average

4

value based of information from a single point then may be inaccurate. Multiple measurements in various locations can reduce this issue but a single measurement method is more desirable. Spectroscopic techniques then become a viable alternative to probing.

The first of these spectroscopic techniques is laser Differential Absorption Lidar (DIAL) [3]. DIAL incorporates a pulse laser operating at two wavelengths, one strongly absorbed and the other weakly absorbed by the gas species of interest. Light backscattered off the gas species is measured as an absorption spectrum. Concentration distribution along the light path are calculated by referencing the pulse time and the light absorption information. The active interrogation of ground level energy state, where the population distribution is highest, provides chemical concentration detection limits down to an order of parts per billion at stand off distances of several hundred meters. With the addition of a scanning telescope/mirror, one DIAL system can map out a 2D slice of an area in question providing a spatial map of species concentrations. This makes DIAL an excelent tool for the detection of single chemicals in combustion sources. The disadvantage of DIAL results from a common trade-off. The narrow laser line shape used to accurately interrogate an absorption energy of a chemical also makes DIAL incapable of detecting multiple chemicals simultaneously. As a result, gathering the necessary chemical information needed to determine something such as combustion efficiency requires a tunable laser and several data runs. This process can represent a significant time sink and may also require the use of hazardous chemical dyes.

Open Path - Fourier Transform Spectroscopy (OP-FTS) is a technique that addresses the need for species resolution. Using a broadband source, radiation is sent through the scene toward a corner-cube reflector. The reflection of the radiation source is sent back through the plume and the remaining transmition signal is picked

5

up by a single pixel detector [1]. The advantage of this technique stems from the large range of frequencies the radiation source emits. A wide radiation band can provide absorption information on several different chemicals in a single measurement. This technique is also an active technique, similar to DIAL, so detection of low concentration chemicals is still possible as the energy source is interrogating the ground level. To gain the advantage of multiple species detection however, this technique trades-off spacial resolution as the gathered signal is an average over the entire Field of View (FOV) of the detector. A second issue is the alignment of multiple equipment elements. Holding a corner-cube reflector in position can require a crane and similar to probing, changing winds can push the plume out of the FOV of the radiation source putting the experiment on hold as the equipment is adjusted. Background calibration measurements also require additional data collection away from the plume so this technique is not a true single measurement solution.

2.2   Passive Diagnostic Sensing Techniques

A flaw shared by most active sensing techniques is keeping a wind driven plume in the FOV of the experiment. A solution to this problem is passive detection that relies on the emitting signal of the hot gasses. The signal stands out from the colder background and is detectable from anywhere around the flame without the assistance of reflection. IR imaging cameras with rotating narrow band-pass filters can provide passive spatially resolved information of a select few species but the quality of this information is usually poor. The most common passive method is Fourier Transform infra-red Spectroscopy (FTS). Aligning the FOV of the spectrometer with a portion of the combustion source with elevated temperatures provides ample emission signal from the hot gas [2]. FTIR detectors also provide a similar broad band detection range capable of picking up emission from several combustion species in one mea-

6

surement [2]. The ease of alignment along with broadband detection does comes at a cost. FTIR still does not provide spatial information, but rather an average over the entire field of view. Additionally, a separate measurement away from the flame is necessary to measure any signal contribution associated with atmospheric path radiance and solar scattering. Most importantly, the passive nature of the technique detects energy released from relaxations to lower energy states from energy states with much lower population than the ground level. This limits the sensitivity for low concentration species and the emissions also become less detectable as they cool, limiting the effective detection area of this technique.

2.3 Imaging Fourier Transform Spectroscopy

In recent years, the development of IFTS has provided a unique and powerful tool for passive remote sensing. IFTS devices pair an IR camera with a Michelson interferometer yielding both broad spectrally and spatially unique data. The addition of the multi-pixel focal plane gives IFTS the spatial resolution standard FTIR techniques lack. Scene imaging capabilities also provide the unique capability of choosing a FOV that includes a small portion of the background. This allows the camera to capture information on the background in the same measurement as the scene of interest making IFTS a true single measurement tool. As with all passive emission detection techniques however, IFTS still suffers from poor sensitivity for species with low concentrations or for species that have relatively weak emission signatures. Despite this the capabilities of this tool have already been proven in combustion settings [4, 5]. Gross et al. successfully estimated effluent concentrations and temperature of an industrial smokestack plume using the Telops Hyper-Cam and a single-layer radiative transfer model [4]. This single-layer model assumption was checked by examination of the variation in column density and temperature with location throughout the

7

plume, a check made possible through the spatial resolution provided by the FPA. Estimated CO_2 and SO_2 volume fractions, found to be 8.64±0.43 % and 380±23 ppm respectfully, compared favorably with *in situ* measurements of 9.4±0.03 % and 383±2 ppm [4]. The work done in this thesis relies heavily on methods introduced in the work by Gross et al.This work was advanced by J. L. Harley to include mass flow rates of smoke stack effluence [5]. IFTS provided accurate spectral information and the spatial detection ability of the camera allowed changes in total intensity to be mapped and followed across the FOV. This mass flow rate detection, measuring 13.5±3.78 kg/s of CO_2 and 71.3±19.3 g/s of SO_2, also compared well with *in situ* of 11.6±0.07 kg/s of CO_2 and 67.8±0.52 g/s of SO_2 [5].

2.4 Laminar Flames

To validate IFTS as a useful tool for CD it is important to start by investigating an uncomplicated combustion source. The New Oxford American Dictionary defines laminar as "A flow taking place along constant streamlines; not turbulent." Laminar flames are designed to have minimal turbulence in the chemical flow field during the combustion process. The relative simplicity of this flow field is the central reason a laminar flame was chosen for this work. Laminar flames are also a widely used tool in the combustion diagnostics industry.This work utilizes a Hencken burner laminar flame. The Hencken burner traditionally provides a calibration reference for laser diagnostic and physical probe techniques such as OH-Absorption, OH - Planar Laser Induced Fluorescence (OH-PLIF) and Coherent Anti-stokes Raman Spectroscopy (CARS) [6, 8, 9, 10, 11]. This large dataset of accepted research available for comparison solidifies the Hencken burner as an ideal flame in the validation of IFTS as a CD tool.

2.5 Meyer et. al.

A paper by Meyer et. al. proved particularly useful to this work [6]. In his work, Meyer develops a high-speed UV absorption sensor for OH based on sum-frequency mixing the output of a rapidly tunable distributed-feedback diode laser with the output of a high-power frequency-doubled Nd:YVO$_4$ laser. This sensor provided quantitative, simultaneous measurements of OH mole fraction and temperature for tracking global instabilities in unsteady flames at rates up to 20 kHz [6]. To achieve temperature and OH mole fraction values, the absorption profile measured by the developed laser system was fit to a Voight profile. Meyer first characterized the performance of the OH sensor in a steady C_2H_4air diffusion flame stabilized over a Hencken burner for a wide range of temperatures and OH mole fractions. These measurements were compared with PLIF, CARS, equilibrium calculations, and a two-dimensional computational fluid dynamics (CFD) code with detailed chemical kinetics. Meyer's use of an identical burner and fuel type allowed for a simple replication of a set of experimental conditions, providing an ideal opportunity for comparison of results. The results of this comparison are presented in Chapters III and IV.

9

III. Mid-wave IFTS measurements of a laboratory-scale laminar

3.1 Abstract

A passive remote sensing technique for accurately monitoring the combustion efficiency of petrochemical flares is greatly desired. A Phase II DOE-funded SBIR lead by Spectral Sciences, Inc. is underway to develop such a method. This paper presents an overview of the current progress of the Air Force Institute of Technology's contribution to this effort. A Telops Hyper-Cam Mid-wave infrared (MWIR 1800–6667 cm^{-1} or 1.5–5.5 μm) imaging Fourier-transform spectrometer is used to examine a laminar calibration flame produced by a Hencken burner. Ethylene fuel (C_2H_4) was burned at four different equivalency ratios $\Phi = 0.80, 0.91, 1.0$ and 1.25. This work focuses on the qualitative spectrally-resolved visualization of a Hencken burner flame and the spatial distribution of combustion by-products. A simple radiative transfer model is then developed and fit to a single-pixel spectrum. The flame spectra were characterized by structured emissions from CO_2, H_2O and CO. For the $\Phi = 0.91$ flame, the spectrally-estimated temperature was $T = 2172 \pm 28$ K at a height 10 mm above the burner, a favorable result compared to OH-absorption measurements ($T = 2226 \pm 112$ K) made on an identical flame. H_2O and CO_2 mole fractions across the flame at the same height of 10 mm were measured to be $13.7 \pm 0.6\%$ and $15.5 \pm 0.8\%$, respectively.

3.2 Introduction

Flaring is a widely used technique for the conversion of flammable gases into combustion byproducts. Under ideal conditions, all carbon and hydrogen in the waste gas has been converted to CO_2 and H_2O. When the combustion is inefficient, particulate material and highly-reactive volatile organic compounds (HR-VOCs) form and

10

are released into the atmosphere posing environmental and health risks. If properly maintained flaring can sustain levels of combustion efficiency[1](CE) greater than 95% [1, 2, 3], however a small drop in CE could represent a large release of HR-VOCs into the atmosphere. Modern flares are built with in-situ CE measurement systems but retrofitting older systems comes at a high cost. Point-sampling methods are highly accurate, but such methods are impractical to implement on a large scale [7]. Spectral techniques such as Ultraviolet Differential Optical Absorption Spectroscopy (UV-DOAS), Laser Differential Absorption Lidar (DIAL), Open-Path Fourier-Transform Infra-Red (OP-FTIR) spectrometry and standard Fourier Transform Spectroscopy (FTS) [1, 2, 3, 12] have been used successfully for plume monitoring. At a basic level UV-DOAS, DIAL and OP-IFTS all send a tunable range of radiation through the scene and a detector measures absorption features in the remaining signal. This presents the time intensive issue of instrument, retro-reflector and detector alignment. Changing winds can quickly push the plume out of the fixed line-of-sight forcing a reset. Passive FTS measurements do not require a source and instead collect thermally emitted radiation from the flare. However, the lack of spatial resolution can be problematic with a dynamic source, particularly when multiple flares are near one another.

One alternative to these techniques is the use of Imaging Fourier-Transform Spectrometry (IFTS), a tool that has only recently become commercially available. We have previously demonstrated the capability of IFTS to accurately quantify smokestack effluents and mass flow rates [4, 5, 13]. Although flares are more turbulent than smokestacks the data collection and analysis are very similar. A well thought out FOV, one that includes a small view of the background, allows the IFTS to capture both the plume and atmospheric radiance signal in one data acquisition. Even if

---

[1]Combustion efficiency is defined as the ratio of carbon converted to CO_2 relative to the total amount of carbon in the fuel.

wind wanders the plume across the FOV, the imaging capabilities of the Focal Plane Array (FPA) allow for dynamic selection and averaging of pixels corresponding only to points of interest in the flame and plumb. Passive techniques may not have the sensitivity of an active measurement, however, the ability to selectively average pixels can help improve sensitivity without the downside of including non-flare sources.

Spectral Sciences is leading a project in conjunction with The University of Utah and The Air Force Institute of Technology (AFIT) to develop a system for the real-time remote monitoring of CE and HR-VOCs in industrial flares. The University of Utah team will apply their state-of-the-art Computational Fluid Dynamic (CFD) and chemical reaction models to predict flare flow-field parameters including temperature, gas density, and species concentrations throughout the entire flare plume. Spectral Sciences are developing the radiative transfer models necessary to simulate flare plume spectra in the infrared. AFIT is standing up a laboratory scale flare testing facility and will provide temporally and spatially resolved infrared spectra which will be used to validate and improve the reactive-flow CFD and radiative transfer models.

Before this goal can be met in full it is necessary to validate the IFTS as an accurate means of CE detection on a well documented flame source. This work utilized a Hencken burner, a flame source primarily used as a calibration reference for laser diagnostic and physical probe techniques [6, 8, 9, 10, 11]. Temperature and species distributions in Hencken burner flames are well known, providing a substantial set of data to reference and compare any conclusions drawn from IFTS measurements. This paper presents the initial measurements made by our Telops MWIR Hyper-Cam IFTS of a Hencken burner laminar flame source burning an ethylene flame at various equivalency ratios with a goal to probe the data provided by the IFTS for relevant information useful to the eventual measurement of CE.

3.3 Experimental

3.3.1 Calibration Flame

A Hencken burner was used to generate a partially-premixed, laminar flat flame ideal for developing and testing combustion diagnostics [14]. The burner is designed with a 1" square hastalloy honeycomb burner surface with stainless steel hypodermic fuel tubes. An image of the burner is provided in Figure 1. The tubes are uniformly distributed throughout one-fourth of the honeycomb holes. The oxidizer, lab air during these experiments, flows around the tubes and exits out of the remaining three-fourths of the honeycomb holes. Surrounding the inner square is an inert gas co-flow section used to isolate the flame from the surrounding air. Additional information on the burner can be found in the literature [14, 15, 16]. All gas flows were regulated using MKS 1480A ALTA^{TM} mass flow controllers. These controllers have accuracy to 1% of set point up to 30 Standard Liters Per Minute (SLPM) of N_2 equivalent. The controllers were operated using a MKS model 247D four channel power supply and digital readout. A Bios, The Definer^{TM} 220 positive displacement volumetric flow meter was used to measure flow exiting the Hencken burner prior to ignition to ensure an agreement with the desired flow rates at the mouth of the burner. The standard reference point for the MKS and the Bios equipment is $0°$ C.

Experiment 1 (Figure 2, A) consisted of three measurements, each with the Hencken burner set to a different equivalency ratio listed in Table 1. Here the equivalency ratio Φ is defined by the actual fuel to oxidizer ratio relative to the stoichiometric fuel to oxidizer ratio

$$\Phi = \frac{n_f/n_{O_2}}{(n_f/n_{O_2})_{st}} = 3 * \frac{\mathrm{f}_{C_2H_4}}{0.21 * \mathrm{f}_{air}} \tag{1}$$

where $\mathrm{f}_{C_2H_4}$ and f_{air} are the fuel and air flow rates given in Table 1. The 0.21 value

13
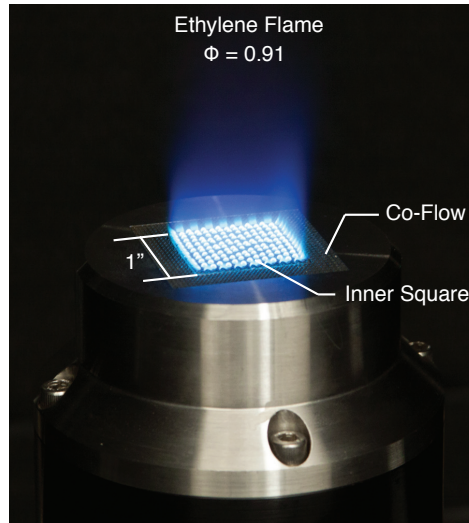
Figure 1. Photograph of a Hencken burner producing an ethylene flame with an equivalency ratio of $\Phi = 0.91$.

is the fraction of oxidizer, O_2, in air and the factor of 3 is a result of the balanced stoichiometric equation for combustion $C_2H_4 + 3O_2 \rightarrow 2CO_2 + 2H_2O$. These changes in equivalency ratios are intended to stimulate visual and spectral differences in the flame detectable to the Telops camera. Nitrogen was mixed into the air flow prior to the Hencken burner in quantities that preserved the volumetric flow rate of the system at 18 SLPM. No co-flow nitrogen was used in these first three trials. This is not the standard method of practice for a Hencken burner. However, the nitrogen co-flow extinguished the flame when $\Phi = 0.8$ so all trials were performed without it. An average ambient temperature of $25.7\,^{\circ}\text{C}$, pressure of 977.9 hPa, and humidity of 46.0% were measured in the lab during this experiment using a Kestrel^{TM} 4000 Weather Meter.

A second experiment (Figure 2, B) was designed to reproduce an ethylene flame characterized by OH-absorption measurements made by Meyer et. al.,[6] the flow rates for this trial are also listed in Table 1. Reproduction of a similar flame provided a point of comparison between spectrally estimated temperature and OP-absorption temperature measurements. Nitrogen listed for this trial does represent a co-flow

14
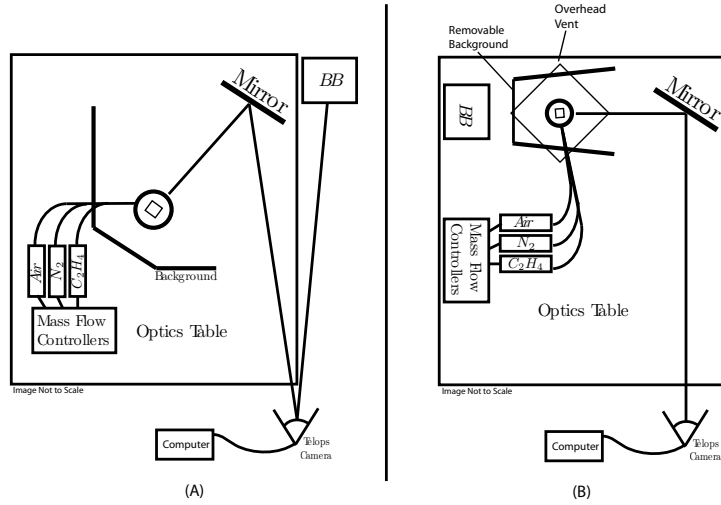
Figure 2. *(A)* **Schematic of experiment 1 setup.** *(B)* **Schematic of experiment 2 setup**

value sent around the flame, no additional nitrogen was added to the air mixture. The flow value of 12.0 was chosen to match the exit velocity of the flame. It should be noted that a separate but dimensionally identical Hencken burner was used for this trial. An average ambient temperature of 24.8° C, pressure of 980 hPa, and humidity of 37% were measured in the lab during this experiment using a Kestrel^{TM} 4000 Weather Meter.

Table 1. Flow values for each trial. Nitrogen added in trials 1 and 2 was mixed with the air stream. Nitrogen added in trial 4 represents the volume of co-flow around the flame.

	Trial #	Fuel [slpm]	Lab Air [slpm]	Nitrogen [slpm]	Equivalency Ratio Ø
Experiment 1	1	0.95	10.91	6.14	1.25
	2	0.95	13.65	3.40	1.00
	3	0.95	17.05	0	0.08
Experiment 2	4	0.78	12.2	12.0	0.91

15

3.3.2 Imaging Spectrometer

A Telops, Inc. (Qubec, Canada) MW-E imaging Fourier-transform spectrometer was used to measure spatially-resolved Mid-Wave Infra-Red (MWIR, 1.5-5.5 μm) spectra. The Telops MWIR IFTS pairs a Michelson interferometer with a 320x256, Sterling-Cooled Indium Antimonide (InSb) focal plane array (FPA). The resolution of the Michelson $\delta\tilde{\nu}$ is variable from 0.25 cm^{-1} to 150 cm^{-1} and is dependent on the Maximum Optical Path Distance (MOPD), $\delta\tilde{\nu} = 0.6/MOPD$. An internal HeNe laser reference triggers an image capture every 632.95 nm. The InSb detector has a sensitivity range of 1800–6667 cm^{-1} (1.5–5.5 μm). Additional details on the Telops IFTS can be found in the literature [17, 18].

During the first three trials the FPA captured images with a 20μs integration time on a 230x64 sub-window, reducing acquisition time and focusing the view on the flame. An internal neutral density filter was activated to prevent camera saturation. The burner was a distance of 3.4 meters away with each pixel corresponding to an area of 1.21x1.21 mm^2. The spectral resolution was set at 1 cm^{-1} to allow for detailed spectral information without slowing down data acquisition. At this resolution a full interferogram cube is gathered every 2.4 seconds with a total of 18,958 images. Note the sizable difference in camera frame rate (7.8 kHz) and the the interferogram cube rate (0.41 Hz). Although the Telops is equipped with two blackbody calibration sources, only one was used. One on-board blackbody was used as a low temperature source and an external 6 square blackbody placed 1.5 m from the camera was used as a high temperature source. The external source was used because the radiance level of the high temperature built in blackbody was lower than the radiance level of the scene. The low temperature source was set to 90°C and the external source was set at 500 ^{o}C. The flame exhibited intensity fluctuations during single interferometric measurements. To mitigate this "source noise" 1000 interferograms were averaged.

16

For the second experiment the line-of-sight distance was reduced to 3 meters, a result of the placement change of the external blackbody source, for a pixel spatial resolution of 1.18x1.18 mm^2. The neutral density filter was removed and the integration time was reduced to $10\mu s$ along with an improvement in spectral resolution to 0.75 cm^{-1}. At this resolution a full interferogram cube is gathered every 2.9 second with a total of 25,278 images. The camera frame rate is then 8.6 kHz and the the interferogram cube rate is 0.34 Hz. An external 12" square blackbody set at 535°C and 450°C was used to calibrate the instrument so that raw spectrum could be converted to radiance units. Calibration consisted of a standard two-point, linear correction [19] with a Hann apodization function applied to the data to minimize any ringing effects. Additional details on the calibration process can be found in Appendix C. A single external blackbody source insures the calibration path length is the same for both temperature acquisitions and is similar in atmospheric path length as the signal from the flame. It also removed the need to rotate the camera between calibration and flame measurements. 500 interferograms were averaged to mitigate source noise.

3.4 Theory

3.4.1 Spectral Model

For an ideal interferometer, the recorded intensity $I_{i,j}$ as a function of optical path difference (x) at a given pixel in the detector with coordinates i and j can be described by

$$I_{i,j}(x) = \frac{1}{2} \int_0^\infty [1 + \cos(2\pi\tilde{\nu}x)]G(\tilde{\nu})L_{i,j}(\tilde{\nu})\mathrm{d}\tilde{\nu} = I_{DC} + I_{AC}(x). \qquad (2)$$

Here, $G(\tilde{\nu})$ accounts for the instrument response, including the spectral quantum efficiency of InSb and $L_{i,j}(\tilde{\nu})$ represents the spectrum of the scene [20]. Assuming

17

a static scene, the intensity can be broken into the broadband spectrally-integrated signal I_{DC} and a modulated component $I_{AC}(x)$. A Fourier-transformation of the modulated intensity, $Y_{i,j}(\nu) = F\{I_{i,j}(x) - I_{DC}\}$ along with a two point calibration[19] will yield the radiance spectrum $L_{i,j}(\nu)$.

This work makes the assumption of homogeneity in the temperature and concentrations along the line of sight. With this assumption the spectral radiance $L(\tilde{\nu})$ from a non-scattering source in local thermodynamic equilibrium can be approximated by

$$L(\tilde{\nu}) = \tau(\tilde{\nu})\varepsilon(\tilde{\nu}, \xi_k)B(\tilde{\nu}, T) \tag{3}$$

where $B(\tilde{\nu}, T)$ is Planck's blackbody radiance at a temperature T modified by the gas emissivity $\varepsilon(\tilde{\nu}, \xi_k)$. Here, $\tau(\tilde{\nu})$ represents the transmittance of the atmosphere between the flame and instrument. The spectral emissivity is related to the gas mole fractions ξ_k through the relationship

$$\varepsilon(\tilde{\nu}, \xi_k) = 1 - \exp\left(-Nl\sum_k \xi_k\sigma_k(\tilde{\nu}, T)\right) \tag{4}$$

where $N = P/(k_BT)$ is the total gas number density, l is the path length through the flame and σ_k is the Boltzmann-weighted absorption cross-section for species k. This model also simplifies the actual radiative transfer problem by neglecting sources of radiation behind and in front of the flame. In the spectral window of 3100 cm^{-1} to 4500 cm^{-1} the contribution of signal from room temperature background radiation is negligible compared with the radiance from the flame. Using information found in the high-temperature extension of the HITRAN database[21, 22], Equations 3 and 14 can be used to generate a model for the expected radiance of the scene. Absorption cross-sections for H_2O and CO_2 are computed using Line-by-Line Radiative Transfer Model [23] and the spectral line parameters from the high-temperature extension of

the 2004 HITRAN database. Details about this model have been reported [4] and an additional discussion is presented in Appendix D.

3.4.2   High-speed Imagery

The Michelson encodes spectral information by modulating each wavelength of light ($\nu = 1/\lambda$) at a difference frequency $f = \nu * V$, where V is the mirror scan velocity. The quantum efficiency of the detector has a lower cut-off value of 1700 cm^{-1} so it will not respond to any photons with lower wavenumber values. Spectral information is then encoded via intensity fluctuations above $f = 850$ Hz for trial 1 (V = 0.50 cm/s) or $f = 935$ Hz for trial 2 (V = 0.55 cm/s). Any frequencies lower than these cutoff values correspond to fluctuations in the measured intensity of the scene. Thus, a low-pass filter, isolating the frequencies below the detector cutoff, applied to an interferogram cube will yield information only associated with the intensity signal I_{DC}. This value at each pixel will map out an image of the scene. Spectrally integrated low-pass interferograms then can be used to image the flame with an effective frame rate of nearly 1 kHz.

3.5   Results and Discussion

3.5.1   Flame Imagery

Figure 3 provides imagery created using the low-pass filtering technique described above. Pictured are three images for each equivalency ratio flame: A single D.C. intensity level image of the flame, the mean signal after all 1000 cubes in the trial were averaged together, and the Standard Deviation (SD) of a single interferogram cube. Imagery of the mean signal reveal several important things. First the high level of nitrogen added to the $\Phi = 1.25$ flame has a visible effect on the shape of the flame. Low levels of oxygen at the mouth of the burner push the base of the

19

flame higher and the edges of the flame wider producing little signal in the center. This may be a result of additional combustion as atmospheric oxygen is entrained 10-20mm above the burner. These effects are reduced in the $\Phi = 1.00$ flame, as the area of low intensity at the center base of the flame has filled in. The images of the $\Phi = 0.80$ flame shows a narrow, more uniform distribution; a result of no nitrogen addition to the air flow. The single D.C. intensity level images show the dynamic nature of the flame. To the eye, the Hencken burner produces a stationary, laminar flame for all three equivalency ratios. Figure 3 however show similar necks and bulges described by Blunk et al. [11]. These bulges result from the buoyant nature of the flame and entrainment of stagnant room temperature air into the hot exhaust of the flame. The SD profile shows the location of these pulsations, indicating the largest variations in intensity at the edges of the flame. Also noticeable in all three trials is a slightly larger deviation on the right side of the flame. This is possibly the result of small wind currents in the lab or uneven fuel flow through the Hencken burner.
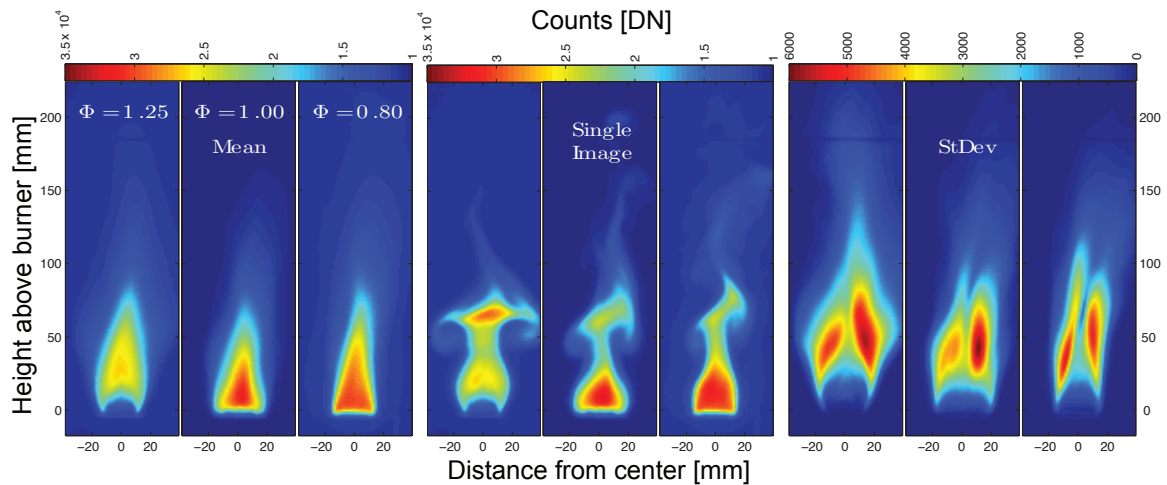
Figure 3. Images of the Hencken Flame for the three different Φ values of experiment 1. The single image for each flame is one intensity image of one interferogram cube. The mean value represents the average over the entire measurement after time-averaging the 500 cubes. The standard deviation represents the deviation over one single interferogram. The images are produced using a Butterworth low-pass filter to retrieve the DC level signal fluctuations.

20

The dynamic nature of the flame visible in the imagery is harmonic in nature. Figure 4 shows the uncalibrated frequency spectrum, or the magnitude of the interferogram's FFT, $Y_{i,j}(\nu)$, taken at pixel (i, j) = (30 mm, 0 mm) for all three equivalency ratios. Both a wavenumber axis and frequency axis are provided[2]. The interferogram in Figure 4 shows the sizable intensity oscillation on which the high-frequency spectral information rides. Examination of the low-frequency spectral intensities (see inset plot in the bottom panel of Figure 4) reveals intense features at 10.1 Hz for $\Phi = 1.25$, 17.5 Hz for $\Phi = 1.00$ and 12.5 Hz for $\Phi = 0.80$ corresponding to the harmonic pulsations of the flame. These features are associated with the resonance phenomena of non-premixed buoyant flames. A similar work done by Kostiuk et. al. [24] utilized a 25 mm diameter tube and setting consisting of 0.3 L/s of fuel flowing at a rate of 1 m/s with an equivalency ratio of $\Phi = 1$. This setup produced a calculated Reynolds number of 1326 and a flickering frequency of 15.46 Hz. In this experiment the $\Phi = 1$ trial was also performed at a 0.3 L/s and 1 m/s flow rate and the Hencken burner has a similar 1 diameter burner opening. The calculated Reynolds number for Trial 1 is 1385 and has a flicker frequency value of 17. 5Hz. These values compare well, within 2 Hz, and differences in diameter shape or flame temperature may account for the difference. Understanding the flicker frequency and why it changes with Φ is not a focus of this work. However, with all other flow conditions being the same, it is believed that the flickering frequency is dependent on the flame temperature, which is dependent on Φ [6, 25, 24, 26]. Future work will be done to investigating a relationship between Φ, temperature and the flicker frequency.

Mitigating source noise by averaging 500 or 1000 interferogram cubes, each with these harmonic fluctuations in D.C. signal level, raises some concern. Each cube will

---

[2]The IFTS camera is triggered to capture an image every zero crossing of the HeNe metrology signal. Thus, this system samples on a fixed OPD grid and not on a fixed clock cycle. Small fluctuations in mirror velocity will introduce subtle errors in frequency analysis.
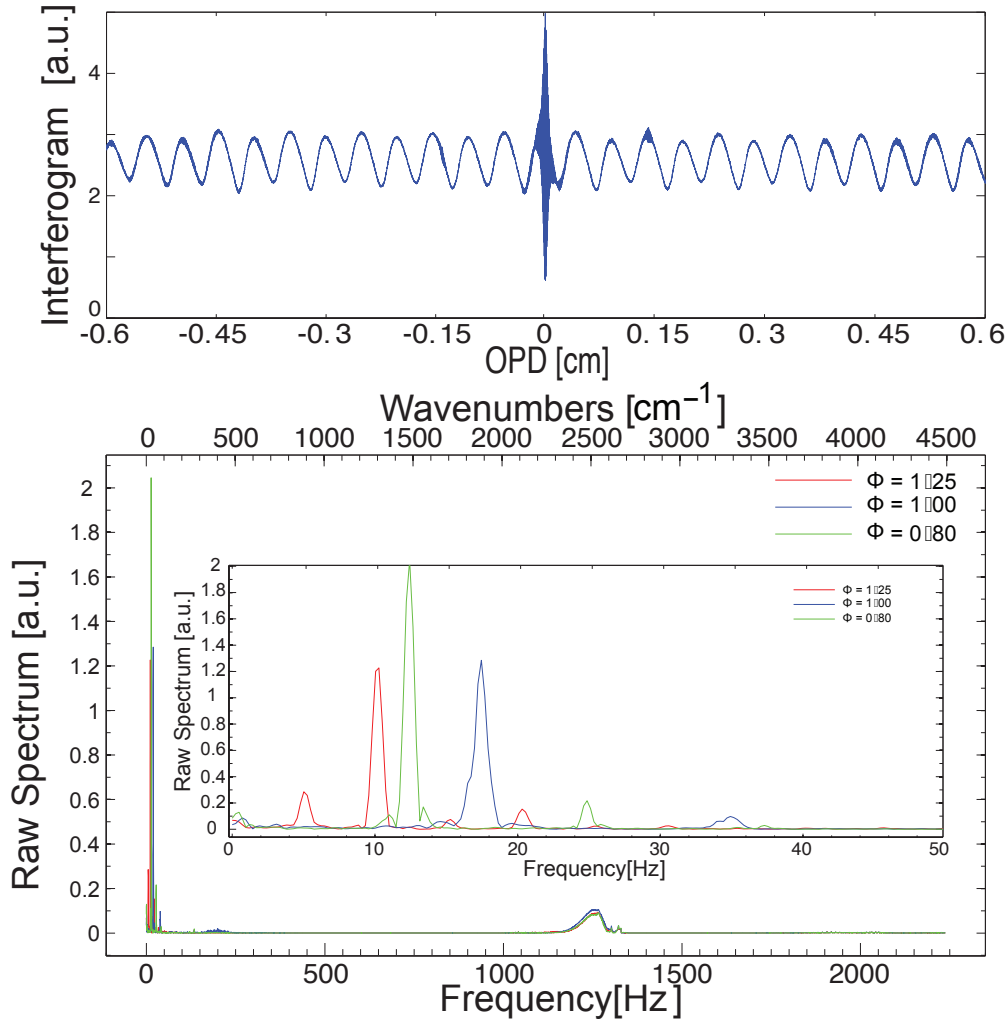
Figure 4. *Images:* (1) A raw interferogram generated from the (i, j) = (30 mm, 0 mm) pixel of a single cube of the $\Phi = 1.25$ flame. (2) Raw frequency spectrum taken at pixel (R, C) = (40, 33) of all three trials in experiment 1. *Inset Image:* An enhanced look at the low frequency flicker information.

have a random starting phase to this fluctuation so an average over 1000 cubes will wash the D.C. level fluctuations out. A theoretical trial was done to investigate the effect this averaging has on the higher frequency spectral line-shape. 1000 interferograms encoded with spectral information created from the HITRAN database were created, each with a harmonic temperature fluctuation. The frequency of this fluctuation was set at 17 Hz and the amplitude of the temperature range was 1650 K to 1850 K. A Fourier transform of an interferogram corresponding to the mean temperature of the 1000 cubes was then compared to the Fourier transform of the average of all 1000 interferograms. The results of the comparison are shown in Figure 5. The inset interferograms show the flattening effect of the averaging process but the difference in the resulting spectra is undetectable. From this we can conclude that averaging the harmonic fluctuations of the D.C. signal will not effect the line-shape of the desired spectra and can be ignored with a simple high-pass filter.
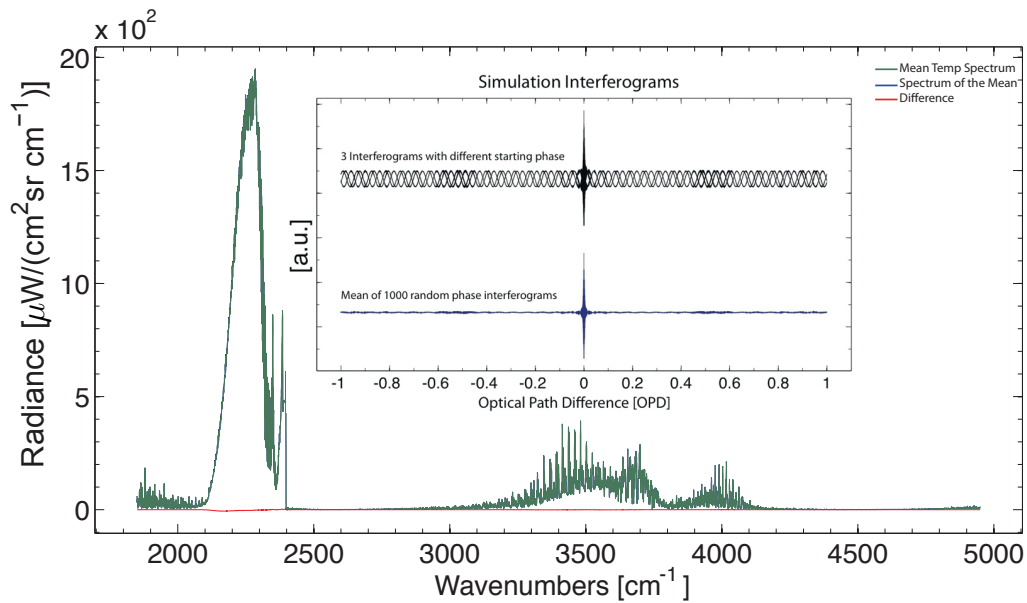
Figure 5. Simulation of the effect of averaging over 1000 interferograms each with a random starting phase for a harmonic 17Hz, 200 K fluctuation in signal level.

3.5.2 Flame Spectra

Figure 6 shows the mean spectra of all trials in Experiment 1 at the pixel (i, j) = (30 mm, 0 mm). Along with the measured spectra are models of CO_2, CO and H_2O as well as the transmission function of the atmosphere generated using the spectral model described above, with estimations for the flame temperature and Volume Mixing Fraction (VMF). Noticeable important features of the spectrum include a fundamental vibrational mode (asymmetric stretch) of CO_2 centered around 2280 cm^{-1}. A portion of this structure is absorbed by atmospheric CO_2 between the flame and the sensor. The P-branch of the CO spectrum just at the left base of the CO_2 feature is also prevalent. Highly structured features between 3100 cm^{-1} and 4150 cm^{-1} are a result of water emission including vibrational levels $\nu_1\nu_2\nu_3$: 001→000, 100→000, 020→000, 011→010, 110→010, and 030→010 again with some absorption from atmospheric water along the line-of-sight. These structured features also ride on top of a broad CO_2 feature in that area.

Detecting differences in these key spectral features is a requirement for combustion diagnostics. Figure 6 shows that differences in the spectra between the three trials is noticeable. The $\Phi = 1.25$ shows a much stronger CO feature than the other two trials which is expected given that the fuel:air ratio does not permit complete oxidation of the carbon in the fuel. Also differences in the width of the CO_2 feature in each trial points to difference in flame temperature as the width of spectral features are proportional to temperature. The overall concentration of CO_2 along the line of sight may be different between each flame so no direct temperature comparison should be made without fitting the data to a model accounting for mole fraction and temperature.

Figure 7 also demonstrates the Telops MW-IFTS' ability to detect changes in the spectrum throughout the same flame. Figure 6 shows that the $\Phi = 1.25$ flame is the

24
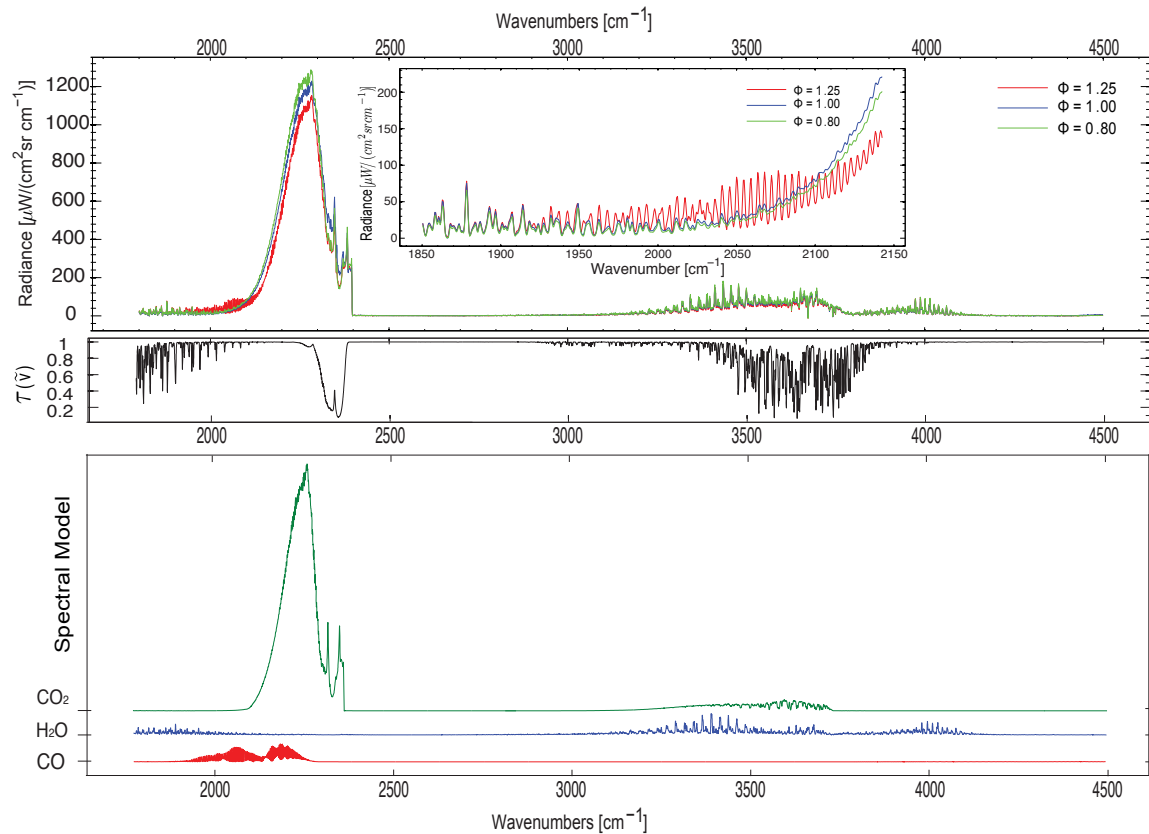
Figure 6. Top panel: Single-pixel spectral radiance of each flame in experiment 1, pixel (i,j) = (30 mm, 0 mm). Middle panel: Atmospheric transmittance profile for the 3.4 m observation path based on measured meteorological conditions Bottom panel: Relative emissivity curves for CO_2 , CO and H_2O (offset for clarity) at the adiabatic flame temperature. Models were created using LBLRTM and HITEMP HITRAN database.

most interesting spectrally, as the chemical features for CO are the most pronounced in this flame, so future analysis in this paper will utilize this flame. The three pixels displayed represent points that are directly in the center, on the edge and at the top of the $\Phi = 1.25$ flame. The spectrum have been peak normalized to minimize column density effects. There are several immediately evident differences in the spectrum across the flame. The inset image in Figure 7 shows a much larger CO feature in the center of the flame than on the top or edge. This points toward incomplete combustion, unlike the top and edges of the flame where excess oxidizer entrained into the flame have completed the combustion. The CO_2 spike is also widest at the center pixel where temperature is largest. A change in the relative intensities of the major CO_2 and H_2O features is evident as well. Despite the CO_2 spike being peak normalized, the hot water spikes around 4000 cm^{-1} are not the same height, pointing to a grating in the ratio of hot CO_2 and H_2O. Spectral intensity is a function of species concentration, temperature and path length all of which are expected to change from the center to the edges as the chemical combustion reaction unfolds so no quantitative comparison should be made. However this would seem to show that a well developed spectral model could glean valuable quantitative information on how the chemistry of the flame changes spatially. Appendix D gives a short discussion on the effects temperature and concentration changes have on a spectrum. An understanding of these effects should provide insight into the results discussed above.

The spatial distribution of relative species concentrations can be qualitatively visualized by examining images and ratios of appropriate band averaged radiance. Choosing the bands appropriately is important to preserve concentration information. The range of 1850 – 2338 cm^{-1} captures the entire CO_2 feature, the range of 1850 – 2143 cm^{-1} captures the entire P-branch of the CO feature and the range of 3100 – 4150 cm^{-1} captures all H_2O features. Although there is some overlap be-

26
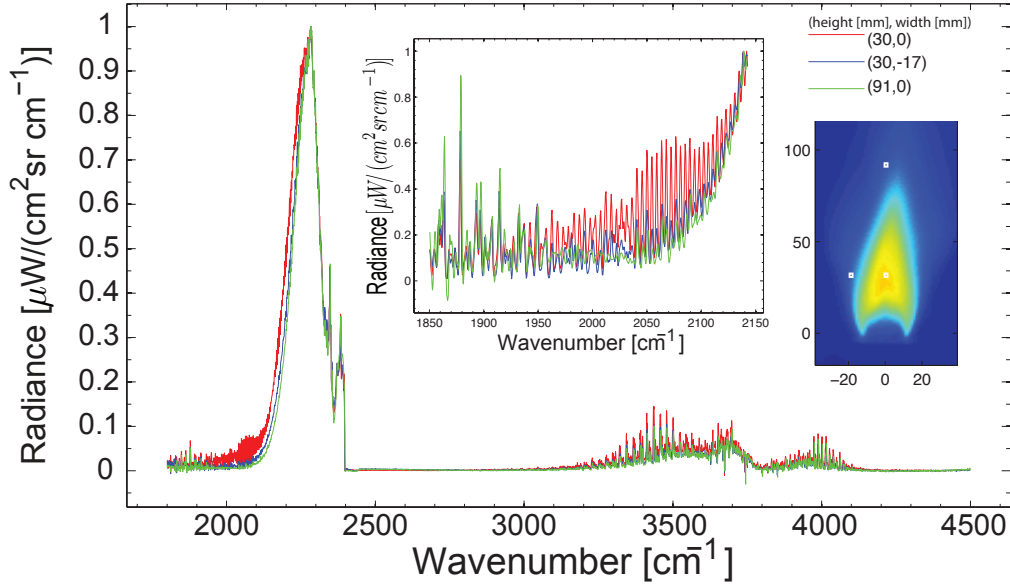
Figure 7. Spectrum for several interesting pixels across the time averaged $\Phi = 1.25$ flame. *Inset images*: **A close view of the CO feature and an image of the flame with pixel locations are provided for clarity.**

tween species features the signal will be dominated by the respective species in each range. Without decoupling temperature and species concentration effects, a direct comparison of ratio values is not advised but integrating over these ranges allows for qualitative imagery of species concentrations. Figure 8 (A) shows the band averaged radiance image dominated by CO_2. It is spatially the largest of the band pass images. CO_2 however is naturally present in the atmosphere and excess CO_2 not produced from the combustion process is being entrained into the flow, heated and captured as signal. The areas with high standard deviations shown in Figure 3 represent these areas of entrainment. This is possibly a cause for the gradual drop in concentration at the edges of the flame, giving it a wider appearance. This is a problem also seen in the H_2O band averaged radiance. As observed in Figure 7, the band dominated by CO emission shows high values in the center of the flame. Both at the edges and high above the burner, the CO line heights decrease substantially compared to the nearby

strong CO2 band. This is due to the availability of entrained atmospheric oxygen for oxidation of CO.

The ideal combustion of ethylene gas produces equal parts H_2O and CO_2. Figure 8 shows that the ratio between H_2O and CO_2 stays very uniform across the flame; only changing at the edges where Figure 3 indicates high mixing activity with the surrounding air. Integration limits as well as differences in emissivity values are among the reasons the ratio values are not 1. The ratio between CO and CO_2 is significantly more dynamic showing an almost topographic layering. This ratio image can be thought of as a simple look into the combustion process in the flame. The sharp rise and fall in the ratio value from the base of the flame to the top shows where in the flame the intermediate chemical steps in the conversion of ethylene (C_2H_4) to CO_2 are taking place. Future application of a quantitative model for species mole fraction will provide more meaningful band pass imagery and a more accurate understanding of the dynamic chemistry of the flame.

3.5.3   Quantitative Interpretation via the Spectral Model

The model described by Equation 3 was fit to a single pixel in the $\Phi = 0.91$ flame at a height of 10 mm above the burner using a Nelder-Mead direct search followd by a Levenberg-Marquaardt gradient-based error minimization. Only the portion of the spectrum from 3100 - 3470 cm^{-1} was used in the fit because of the presence of water and carbon dioxide features as well as little interference from atmospheric absorption. Figure 9 shows the model fit and residuals-offset by -50 $\mu W/(cm^2 sr\ cm^{-1})$ for clarity. The residuals show no structure, suggesting the model has no systematic errors and is a good fit. The model temperature at this point compares well with the OH-absorption values measured by Meyer et. al. [6]. At 10 mm above the center of the flame the temperature measured by OH-absorption was 2226±112 K,

28
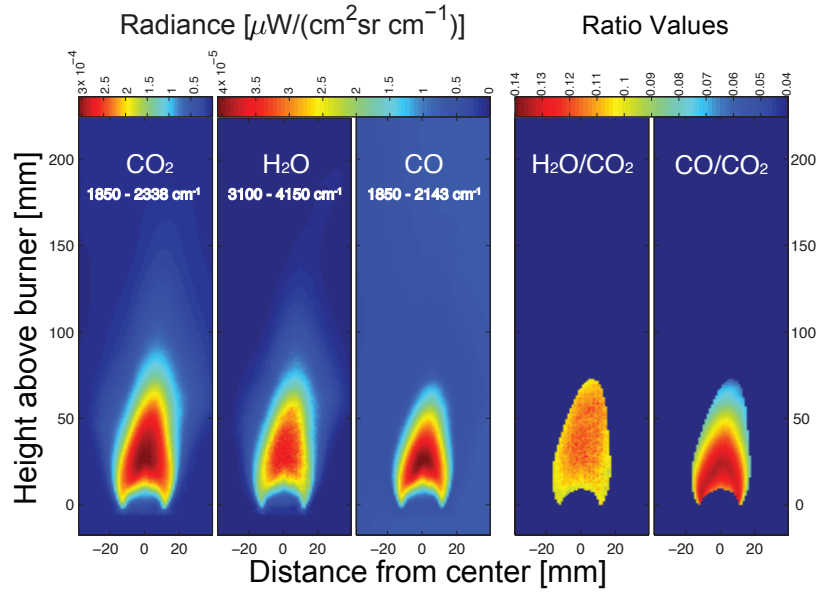
Figure 8. Band pass images of the $\Phi = 1.25$ flame. *Image 1*: Normalized integration over the 1850 - 2338 cm^{-1} CO_2 band. *Image 2*: Normalized integration over the 1850 -2143 cm^{-1} CO band. *Image 3*: Normalized integration over the 3100 - 4150 cm^{-1} H_2O band. *Image 4*: Ratio of the H_2O and CO_2 bands. *Image 5*: Ratio of the CO and CO_2 bands. The ratio images have been windowed according to signal strength to isolate only the flame. This removes color scaling issues caused by the division of numbers close to zero in the background.
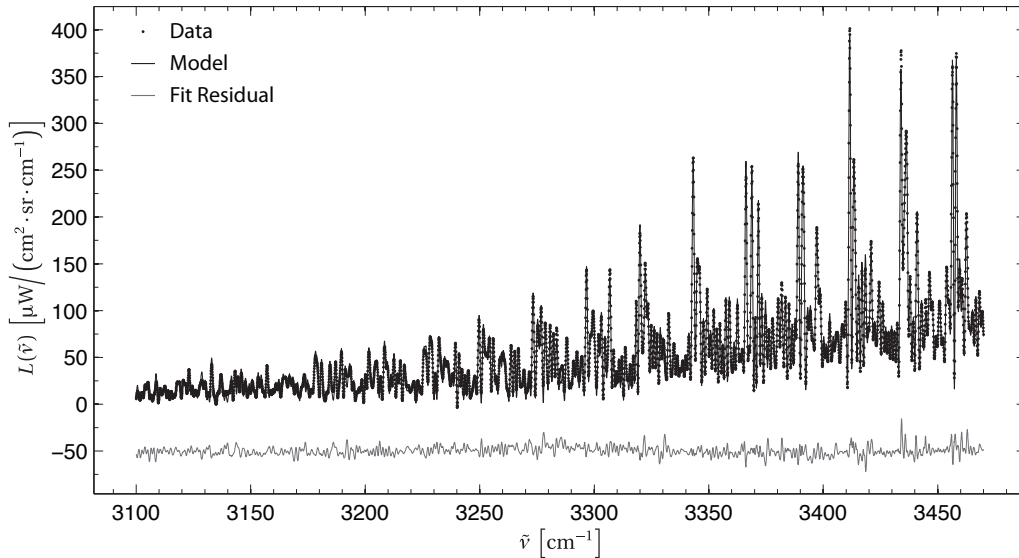
Figure 9. Comparison of model fit (-) to measured (.) $\Phi = 0.91$ flame data taken at flame center 10 mm above the Hencken burner. Fit residuals (data - model) are shown in grey and are offset by $50\,\mu W/\left(cm^2\,sr\,cm^{-1}\right)$ for clarity.

29

and the temperature obtained using IFTS was 2172 ± 28 K. Temperature uncertainty represents a four-fold increase from the regression standard error to account for, in an approximate fashion, systematic errors introduced by the single-layer approximation. systematic errors in assuming a single-layer model. These temperatures agree well and are both lower than the ideal 2302 K chemical equilibrium temperature based on calculations using the NASA CEA code [27]. A lower than ideal temperature is expected as some heat is lost to the burner surface and to entrained air.

The spectral model described by Equation 3 was also used to retrieve H_2O and CO_2 mole fractions at the same point in the flame. H_2O and CO_2 mole fractions were estimated as 13.7 ± 0.6 % and 15.5 ± 0.8 %, respectively. The concentration uncertainties incorporate a 5code values of 11.4% and 11.0% for H_2O and CO_2. This over estimation in mole fraction is still under investigation at this time. Future work will not assume a homogeneous line-of-sight but rather incorporate a layering technique for a more accurate estimation.

3.6   Conclusions

This preliminary analysis of a laminar calibration flame is a first step toward the goal of real-time, continuous monitoring of full-scale industrial flares. These measurements show the visualization of a laminar flame using a mid-IR imaging Fourier transform spectrometer. This investigation demonstrates the potential of IFTS for combustion diagnostics by detecting changes in the spectral information spatially throughout a single flame and over various equivalency ratios. The development of an initial radiative transfer model and exploitation of flame symmetry have made it possible to retrieve temperature and concentration estimates in the flame. Spectrally estimated temperatures agree with those obtained by OH-absorption measurement of a similar flame. Retrieved mixing fractions of H_2O and CO_2 are systematically too

30

large as compared to equilibrium calculations. A spectral model that does not assume symmetry through the flame is in development and should enable more accurate species mole fractions as well as a layered temperature estimate.

IV. Application of an Imaging Fourier-Transform Spectrometer to Determine Two-Dimensional Scalar Values in Laminar Flames

4.1 Abstract

Measurements of scalar values are critical for validating chemical kinetic models, understanding new combustion phenomenon, and verifying numerical simulations. Intrusive based measurement techniques generally can be readily implemented to provide data at a single location. Laser based techniques can provide two-dimensional measurements with high spatial and high temporal resolution through implementation of more elaborate experimental arrangements. In this work an emission based measurement technique is implemented in a simple experimental arrangement to obtain two-dimensional scalar distributions in a laminar flame. A Michelson-based Fourier-transform spectrometer coupled to a mid infrared camera (i.e., 1.5–$5\mu m$) is used to obtain two-dimensional spectral intensity measurements of radiation emitted from water vapor and carbon dioxide. To validate this new technique, measurements are collected from an ethylene (C_2H_4) flame produced by a Hencken burner at an equivalence ratio of $\Phi = 0.91$. A single-layer model is developed to estimate the temperature and H_2O and CO_2 concentrations at varying heights above the burner using spectrally-resolved flame emissions between 3100 cm$^{-1} \leq \nu \leq 3500$ cm^{-1} (2.86 μm $\leq \lambda \leq 3.23$ μm). At the flame center 10 mm above the burner, temperature was estimated as T $= 2172 \pm 28$ K, and this compares favorably with both recently reported OH-absorption measurements (T $= 2226 \pm 112$ K) and equilibrium calculations (T $= 2302$ K). Advantages and limitations of this new technique are discussed.

4.2 Introduction

Scalar measurements in flames are needed for understanding combustion phenomenon, validating chemical kinetic models, and verifying numerical models. Intrusive based measurement techniques, such as thermocouples or gas sampling to a gas chromatograph, are often straightforward to implement at discrete locations. Measurements at multiple locations or simultaneous determination of temperature and species (at a location) can be challenging due to disturbances in the flow. Laser diagnostics, such as planar laser induced fluorescence or Coherent anti-Stokes Raman scattering [28, 29], can provide nonintrusive discrete or planar measurements of temperature and species concentrations. These techniques often require more elaborate experimental arrangements. Infrared emission/absorption spectroscopy measurement techniques are nonintrusive and use tomographic deconvolution processes to determine scalar values [11, 30]. Multiple (independent) line-of-sight measurements are generally collected to obtain the needed spectral and spatial information. This limits the spatial resolution and the ability to capture fluctuations in scalar values at multiple locations. Inverse deconvolution techniques which use spectral measurements collected using Imaging Fourier-Transform Spectrometers (IFTS) are a promising tool for non-intrusively obtaining scalar values in two-dimensions. The utility of IFTS in quantifying species concentrations in a non-reacting turbulent exhaust plume exiting a coal-fired power plant has been demonstrated [4].

This work provides the first spectral radiation intensity measurements of a partially premixed laminar ethylene flame obtained using a mid-IR imaging Fourier-transform spectrometer. The flame was generated using a Hencken burner and matched conditions reported previously. A simple radiative transfer model is developed to estimate flame temperatures and mole fractions of H_2O and CO_2. Spectrally-estimated temperatures agree with previous laser-based measurements of the same

33

flame. Preliminary analysis of the flame is presented. This effort lays the groundwork for developing IFTS into a nonintrusive combustion diagnostics tool for obtaining two-dimensional scalar values.

4.3   Experimental Arrangement

A Telops Hyper-Cam MW-E imaging Fourier-transform spectrometer was used to measure spatially-resolved Mid-Wave Infra-Red (MWIR, 1.5–5.5 μm) spectra of a partially premixed laminar ethylene flame generated by a Hencken burner. The 2.54 cm square burner has an array of fuel tubes arranged in a honeycomb mesh through which the oxidizer flows. The fuel and oxidizer mix shortly above the burner to result in a partially premixed flame. Details regarding the burner are reported in the literature [15]. The IFTS was placed at a line-of-sight distance of 3 m from the flame. Spatial limitations required the use of a mirror (Thor Labs ME8S-G01) while collecting the measurements as illustrated in Figure 10 (a). The Hencken burner was placed in a three-sided enclosure to minimize room disturbances. The flame was produced by flowing 12.2 Standard Liters Per Minute (SLPM) of air and 0.78 SLPM of ethylene through the burner for an equivalence ratio (Φ) of 0.91. These conditions produced a flame which had been previously characterized using OH Planar Laser-Induced Fluorescence (OH-absorption) measurements [6]. A 12.0 SLPM nitrogen co-flow surrounded the flame for enhanced stability. Flow rates were controlled using MKS 1480A ALTA mass flow controllers. Laboratory conditions during testing were steady with a temperature of 298 K, pressure of 980 hPa, and relative humidity of 37%.

The Telops MWIR IFTS mates a 320 x 256 pixel, Sterling-cooled Indium Antimonide (InSb) Focalplane Array (FPA) to a Michelson interferometer. For reference, a Michelson interferometer is depicted in Figure 10 (b). Spectral resolution can be

34
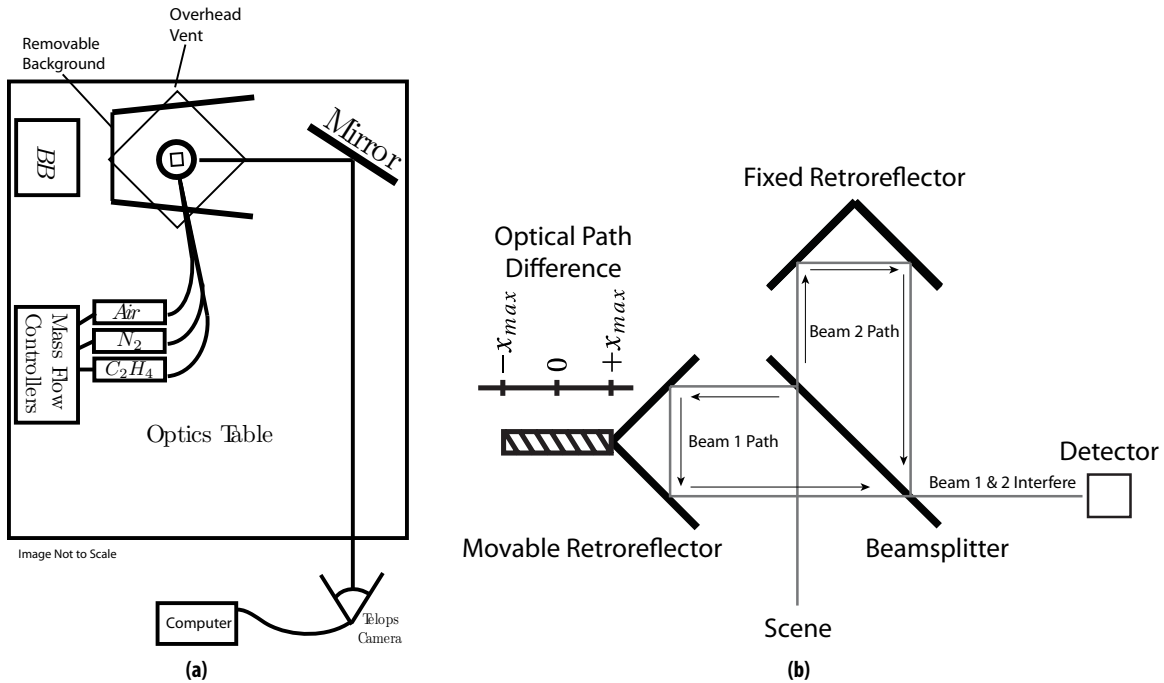
Figure 10. (a) Schematic of experimental setup.(b) Diagram of a Michelson interferometer.

varied from 0.25 cm^{-1} to 150 cm^{-1}. Instrument details can be found in the literature [17, 18]. For this experiment, the FPA captured images with a 20 μs integration time on a 230 x 64 pixel sub-window. The spatial resolution of each pixel was 1.18 mm^2 at the flame. The spectral resolution was set to 0.75 cm^{-1}. This was achieved by continuously scanning the Michelson interferometer at a uniform speed (0.55 cm s^{-1}) to a maximum optical path difference of $\pm$ 0.8 cm with images captured every 632.8 nm. Each interferometric measurement was acquired in just under 3 s and consists of 25,278 images. Note the difference between the camera frame rate (8.6 kHz) and the interferometric cube (i.e., an entire sweep of the spectra) rate (0.34 Hz). Five hundred interferometric cubes of the flame were acquired. The flame exhibited considerable intensity fluctuations throughout single interferometric measurements. The 500 interferograms were averaged to mitigate this "source noise".

Data for radiometric calibration was collected using a 12" square CI Systems

35

blackbody source placed 15 cm behind the Hencken burner. A two-point calibration was performed to remove both system response and instrument self-emission from the raw signal by measuring the blackbody at 450^oC and 535^oC. A diffuse, spectrally-flat black cardboard was placed between the burner and the blackbody to provide a uniform background during flame measurements. Calibrated radiance spectra $L(\nu)$ are reported with units $\mu\,W/(cm^2\,sr\,cm^{-1})$. The spectral variable $\nu = 1/\lambda$ is expressed in wavenumbers with units cm^{-1} and is proportional to frequency.

4.4   Theory

The IFTS records images through a continuously-scanning Michelson interferometer. As the optical path difference (x) between the two beams is varied, the image intensity $I_{i,j}$ varies based on the spectrum $L_{i,j}(\nu)$ in accordance with

$$I_{i,j}(x) = \frac{1}{2}\int_0^\infty [1 + \cos(2\pi\tilde{\nu}x)]G(\tilde{\nu})L_{i,j}(\tilde{\nu})\mathrm{d}\tilde{\nu} = I_{DC} + I_{AC}(x). \qquad (5)$$

Here, i and j refer to the pixel coordinates. $G(\nu)$ accounts for the instrument response, and includes the spectral quantum efficiency of InSb which does not respond to frequencies below approximately 1700 cm-1. For a static scene, the interferogram $I_{i,j}$(x) can be expressed as a constant I_{DC} — the broadband spectrally-integrated signal — and a modulated component I_{AC}(x). The raw spectrum is obtained from the interferogram via Fourier-transformation, $Y_{i,j}(\nu) = F\{I_{i,j}(x) - I_{DC}\}$. A standard calibration [19] yields the radiance spectrum $L_{i,j}(\nu)$. The maximum optical path difference in the instrument is finite, $|x| \leq x_{max}$, and this has an effect equivalent to multiplying the interferogram by a rectangle function of width x_{max}. This limits the spectral resolution, since in the Fourier domain, this is equivalent to convolving the monochromatic spectrum with the instrument line shape function $ILS(\nu) = 2\ x_{max}$ sinc($2\ \pi\ \nu\ x_{max}$).

36

In this work, the flame is assumed to be homogeneous along the line of sight to simplify the development of a model for retrieving scalar values from the measured spectra. In this case, the spectral radiance L(ν) from a non-scattering source in local thermodynamic equilibrium is approximated by

$$L(\tilde{\nu}) = \tau(\tilde{\nu})\varepsilon(\tilde{\nu}, \xi_\kappa)B(\tilde{\nu}, T) \tag{6}$$

where $\varepsilon(\nu,\xi_\kappa)$ is the gas emissivity, which is a function of gas mole fractions ξ_{kappa}, and B(ν,T) is Planck's blackbody radiance at a temperature (T). Here, $\tau(\nu)$ represents the transmittance of the atmosphere between the flame and instrument. This simplified model ignores any background radiation transmitted through the flame. (In the spectral window chosen for analysis, background radiation is negligible.) Convolution with the instrument line shape is implied. The spectral emissivity is related to the gas concentrations and temperature through the relationship

$$\varepsilon(\tilde{\nu}) = 1 - \exp\left(-Nl\sum_\kappa \xi_\kappa \sigma_\kappa(\tilde{\nu}, T)\right) \tag{7}$$

where N = $P/(k_B T)$ is the total gas number density, l is the path length through the flame, and σ_κ is Boltzmann-weighted absorption cross-section for species κ. In this work, a path length of 2.54 cm is assumed based on the Hencken burner geometry. Absorption cross-sections for H_2O and CO_2 were computed using Line-by-Line Radiative Transfer Model [23] using the high-temperature extension of the HITRAN spectral database [21, 22]. Details about this model have been reported [4].

For select pixels, Equation 6 was fit to a spectral window between 3100 cm^{-1} $\leq$ $\nu \leq$ 3500 cm^{-1} with temperature and mole fractions of H_2O and CO_2 as adjustable parameters. This spectral window was chosen as it contains emission from both water and carbon dioxide with minimal attenuation by atmospheric gases. Optimal

37

parameters were determined by minimizing the sum of squared differences between the data and model. This was accomplished using a Nelder-Mead direct search followed by Levenberg-Marquardt gradient-based error minimization.

4.5 Results and Discussion

4.5.1 High-speed Imagery

The Michelson interferometer encodes spectral information via intensity variations (as represented by the cosign term in Equation 5). These variations occur at a frequency greater than 935 Hz, corresponding to the product of the mirror scan velocity (0.55 cm s^{-1}) and the lowest frequency photon (1700 cm^{-1}) that the camera detects. Thus, a low-pass filter can be applied to the interferogram cube yielding moderate-speed imagery with an effective frame rate of nearly 1 kHz. Examination of the low-pass filtered broadband (i.e., spectrally integrated) imagery revealed fluctuations in flame intensity.

The time-averaged flame image is presented in the left panel of Figure 11. Aspects of the dynamic nature of the flame are revealed in the middle and right panels of Figure 11. The middle panel illustrates the difference between an instantaneous and mean flame image, and the right panel presents the standard deviation of pixel intensities. Intensity fluctuations are strongest between 30–90 mm downstream where they can be up to 50% of the mean signal. These fluctuations, which may be due to entrainment of the ambient-temperature N_2 co-flow and possible variations in the fuel and air flow rates, suggest that temperature and mole fractions of H_2O and CO_2 are stochastic variables. The spectra presented in the next section represent an average of the measurements. Since temperature and gas concentrations non-linearly affect the observed radiance, care must be exercised in quantitative interpretation. The spectral analysis presented in this work is primarily focused at 10 mm above the burner where
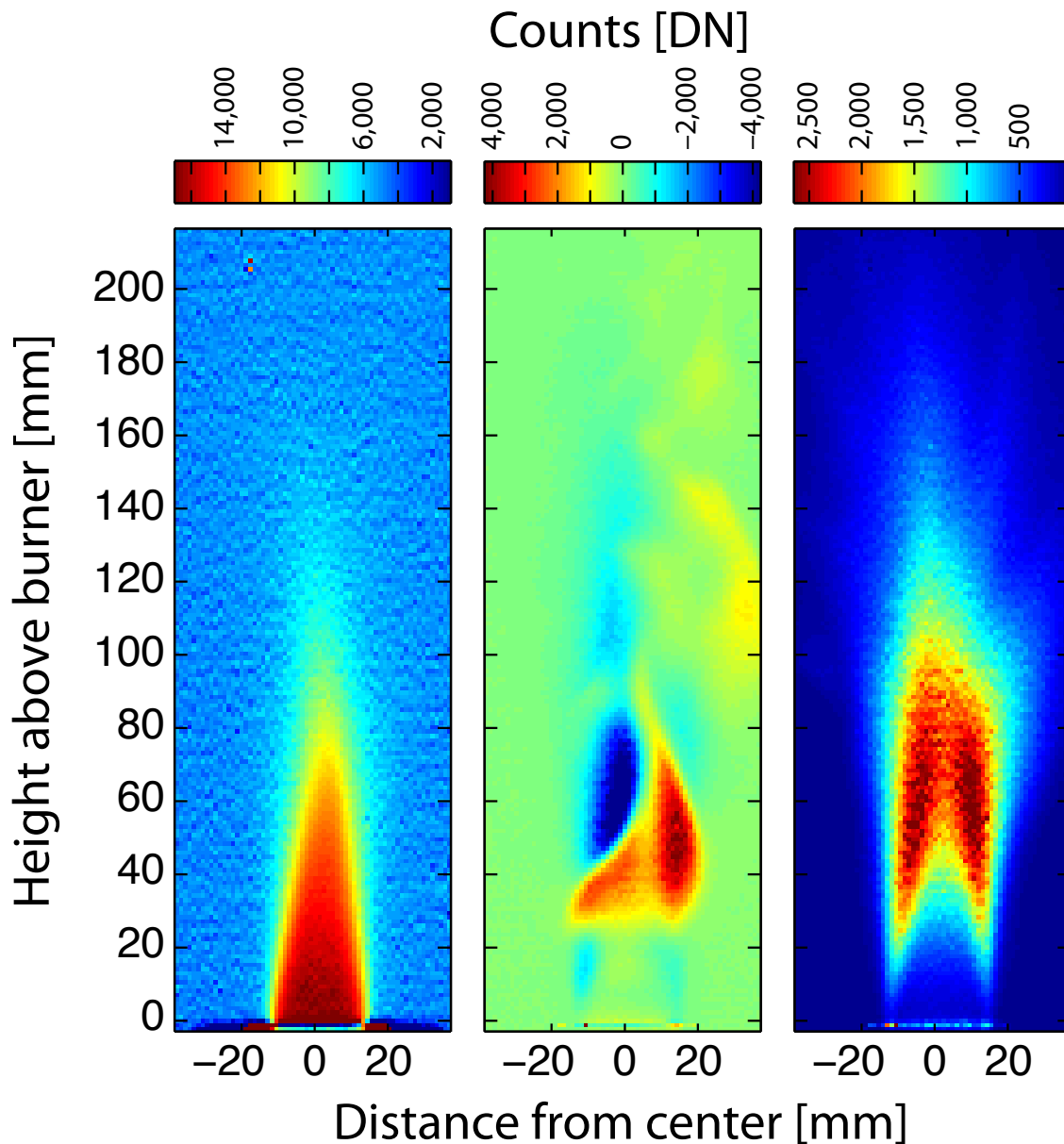
Figure 11. Left panel: Time-average, broad-band intensity image of the ethylene flame immediately above the Hencken burner. Center panel: Difference between an instantaneous flame image and the mean flame image. Right panel: Standard deviation of pixel intensities. Intensities are uncalibrated and reported in raw digital number (DN) counts.

the intensity fluctuations are minimal. At this height, intensity variations were less than 2% of the mean signal, and as a result, fluctuations in temperature and mole fraction are expected to be minimal as well.

Fourier analysis of the time-resolve intensity fluctuation revealed a large harmonic at 18.3 Hz. The cause of this is under investigation. While resonance phenomena in non-premixed buoyant flames are well known [25], the observed pulsation frequency is nearly double that predicted by the empirically-determined relationship relating burner diameter D = 25.4 mm and frequency: $f = 1.68 \times D^{-1/2} \approx 10.5$ Hz. While high-speed imagery analysis is not central to this work, it indicates the versatility of IFTS for combustion diagnostics.

4.5.2 Spectral Analysis

The mean flame spectrum of ethylene 10 mm above the center of the Hencken burner is presented in the top panel of Figure 12. The strongest emission feature is observed at 2250 cm^{-1} and is due to a fundamental vibrational mode (asymmetric stretch) of carbon dioxide. Some of this emission is attenuated due to atmospheric CO_2 between the flame and sensor. Highly structured emission from water is observed between 3000 cm^{-1} and 4100 cm^{-1}, again with some of the signal being attenuated by atmospheric water vapor along the instrument's line of sight. The middle panel presents relative gas emissivity curves for CO_2 and H_2O near ethylene's adiabatic flame temperature (2300 K). Each emissivity profile has been multiplied by the atmospheric transmittance function between the flame and sensor. This transmittance profile was computed using measured meteorological lab conditions and is provided in the bottom panel of Figure 12.

To retrieve path-averaged flame temperatures and water vapor and carbon dioxide concentrations, a small spectral region was chosen for analysis using the radiative

www.manaraa.com
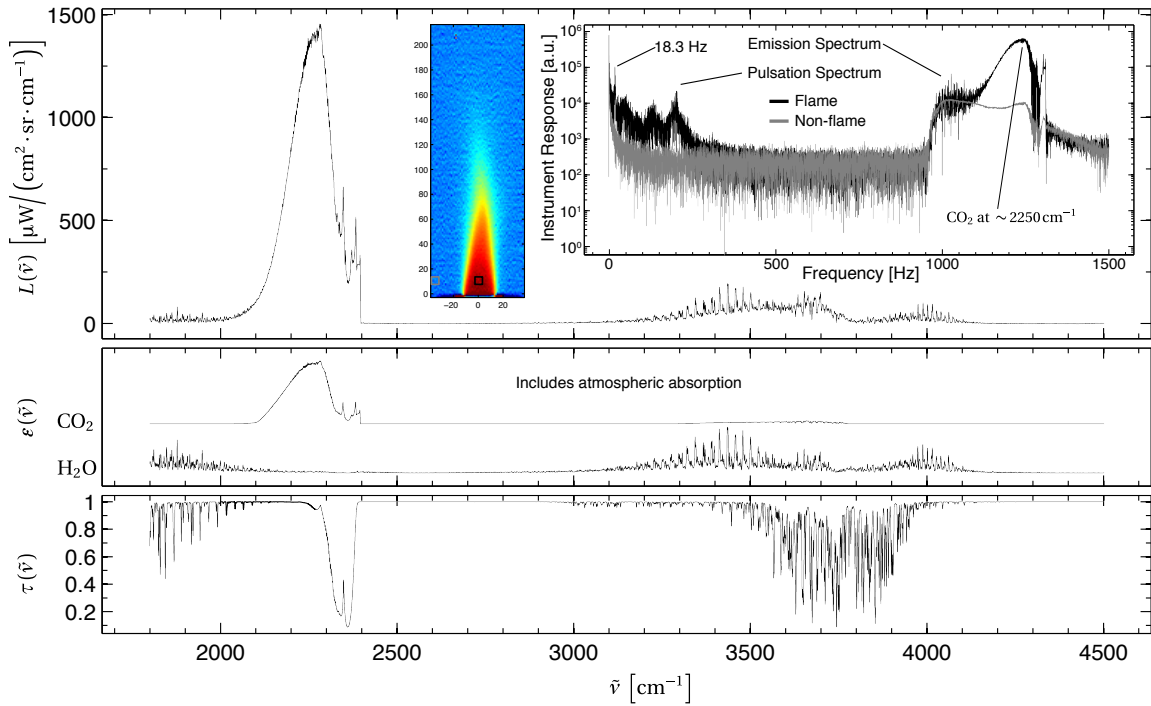
Figure 12. Top panel: Single-pixel spectral radiance of ethylene flame 10 mm above the burner. Black box in inset image indicates pixel location. Inset plot shows corresponding low frequency pulsation spectrum (black) as compared to that from a pixel not imaging the flame (grey). Middle panel: Relative emissivity curves for CO2 and H2O at the adiabatic flame temperature. Bottom panel: Atmospheric transmittance profile for the 3 m observation path based on measured meteorological conditions.

41

transfer model expressed in Equation 6. The model incorporates a computationally-expensive line-by-line calculation. To expedite processing, a small spectral range for analysis is desired. However, the spectral range must contain a distribution of emission lines arising from transitions between a wide enough range of energy levels so that temperature can be reliably estimated. For this purpose, the spectral range of $3100 \text{ cm}^{-1} \leq \nu \leq 3500 \text{ cm}^{-1}$, corresponding to $2.86 \text{ } \mu\text{m} \leq \lambda \leq 3.23 \text{ } \mu\text{m}$, was chosen. Within this range are a large number of H_2O ro-vibrational lines corresponding to transitions between several different vibrational states[1], and as a result, good temperature estimations can be made. Additionally, broadband emission from CO_2 is observed in this region and absorption from atmospheric gases is minimal.

The spectrum and model fit of Equation 6 to a pixel 10 mm above the Hencken burner at flame center are compared in Figure 13. The difference between the model and data are provided—offset for clarity—and indicate that the model captures most of the variation in the data. The fit residuals are unstructured, suggesting that the radiative transfer model describes the data without large systematic errors. For this pixel, the best fit temperature was 2172 ± 28 K and mole fractions of H_2O and CO_2 were estimated as 13.7 ± 0.6 % and 15.5 ± 0.8 %, respectively. The temperature uncertainty has been increased four-fold from the regression's 95% confidence interval in order to estimate the influence of small systematic errors in assuming a homogeneous gas along the line-of-sight[2]. The concentration uncertainties incorporate a 5% path length error. In the absence of path length error, the regression uncertainty in H_2O mole fraction is 0.002%, which is approximately 50 times smaller than that for the CO_2 concentration. This is a result of differences in the emission properties of water

---

[1]In this region, transitions between vibrational levels, denoted v_1 v_2 v_3, include 001→000, 100→000, 020→000, 011→010, 110→010, and 030→010

[2]The arbitrary scaling of temperature uncertainty brings it in line with pixel-wise temperature variations at flame center as discussed shortly. These pixel-wise variations likely give a better estimate the true temperature uncertainty.

and carbon dioxide within this spectral window. A large number of sharp H_2O emission lines of varying amplitudes are present and highly constrain its mole fraction. However, emission from CO_2 is broadband and fairly unstructured in this region, and as a result the retrieved concentration is an order of magnitude less accurate.

The retrieved temperature compares well with temperature measurements of an identical ethylene flame produced by a Hencken burner [6]. At 10 mm above the center of the flame the temperature obtained using OH-absorption was 2226 ± 112 K, and the temperature obtained using IFTS agrees within the reported statistical uncertainty.
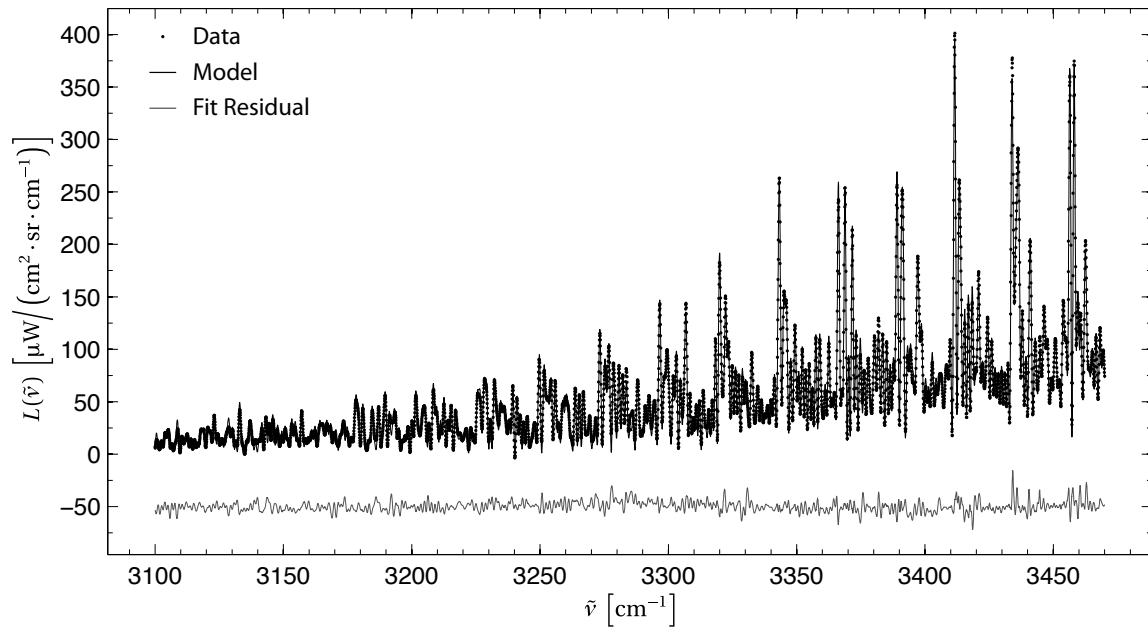
Figure 13. Comparison of model fit (—) to measured (●) ethylene data at flame center 10 mm above the Hencken burner. Fit residuals (data – model) are shown in grey and are offset by 50 μW/(cm2 sr cm-1) for clarity.

Chemical equilibrium temperature is 2302 K and mole fractions of H_2O and CO_2 are 11.4% and 11.0%, respectively based on calculations using the NASA CEA code [27]. Differences between calculated and estimated mole fractions are attributed to

43

uncertainty associated with the path length through the flame, mixing-layer effects that may bias the estimated temperature (which affects the total gas density N), and the unsteadiness of the flame. This is a matter for future investigation.
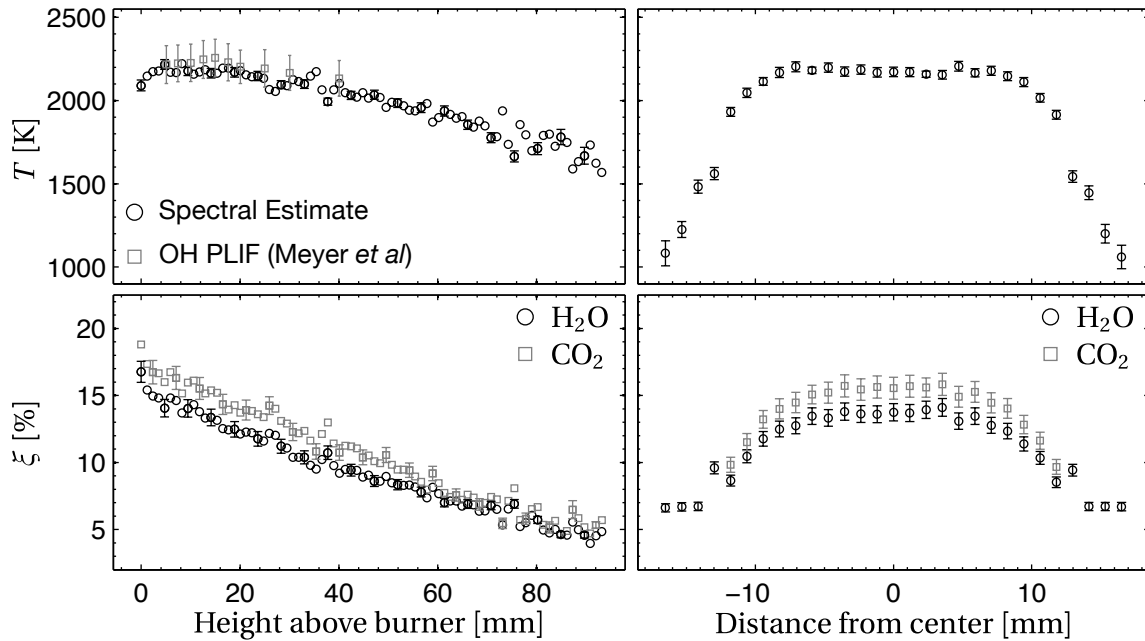
Figure 14. Left-panel: Vertical temperature (top) and H2O / CO2 concentration (bottom) profiles at flame center. Temperature is compared with results from OH PLIF measurements from Meyer et al. Right-panel: Horizontal temperature (top) and H2O / CO2 concentration (bottom) profiles 10 mm above Hencken burner. CO2 concentrations could not be reliably determined at the flame edge and are omitted.

The spectral model was used to retrieve gas temperature, H_2O, and CO_2 mole fractions as a function of height above the burner along the flame centerline. The results are presented in the left panels of Figure 14. The top-left panel compares the retrieved temperatures with the OH-absorption measurements at various heights. The temperatures agree within measurement uncertainties. The temperature follows a gradual decrease with height, and this general trend is expected based on entrainment of the N_2 and surrounding air. The bottom-left panel of Figure 14 shows that the gas concentrations decrease nearly linearly with distance from the burner. CO_2 mole

fractions were consistently higher than H_2O. However, fit uncertainties associated with the carbon dioxide mole fraction were 30–90 times larger than those for water mole fraction.

The temperature and mole fractions of H_2O and CO_2 were determined across the width of the flame at 10 mm above the burner. These results are presented in the right panels of Figure 14. The temperature profile is uniform across the center 18 mm of the flame. In this region, the mean and standard deviation of the temperature are 2168 K and 26 K, respectively. Beyond this center region, the estimated temperature drops by approximately 1000 K over a distance of 7 mm. The radial decay in the mole fractions are similar; however, both exhibited a more gradual decrease near the edge of the flame than the temperature profile. While H_2O and CO_2 mole fractions are independently fitted parameters, they are highly correlated with r^2 ¿ 0.98 in the center 18 mm of the flame. At the flame edge, mole fractions of CO_2 could not be reliably determined. The drop in temperature and mole fractions at either edge suggests a mixing layer width of approximately 7 mm wide at a height of 10 mm above the flame. This will be used to develop a multi-layer radiative transfer model.

4.6   Summary and Conclusion

The measurements represent the first investigation of a laminar flame using a mid-IR imaging Fourier-transform spectrometer. This investigation demonstrates the potential of IFTS for combustion diagnostics. Spectrally estimated temperatures agree with those obtained by OH PLIF measurement of a similar flame. Retrieved mixing fractions of H_2O and CO_2 are systematically too large. Further analysis is required to ascertain if this is due to path length and mixing layer effects.

IFTS offers several unique advantages for combustion diagnostics. First, it is a portable, field deployable piece of hardware that can be set up and collecting cal-

ibrated spectral imagery in less than an hour. It enables the measurement of a moderate resolution spectrum (up to 0.25 cm^{-1}) across a wide band pass (1.5–5.5 μm) so that temperature and multiple species can be monitored simultaneously. Additionally, high-speed imagery can be extracted from the interferometric cube via a low-pass filter, thus enabling additional flow field analysis.

V. Conclusions

IFTS offers several unique advantages for combustion diagnostics. First, it is a portable, field deployable piece of hardware that can be set up and collecting calibrated spectral imagery in less than an hour. It enables the measurement of a moderate resolution spectrum (up to 0.25 cm^{-1}) across a wide band pass (1.5–5.5 μm) so that temperature and multiple species can be monitored simultaneously. Additionally, high-speed imagery can be extracted from the interferometric cube via a low-pass filter, thus enabling additional flow field analysis. By detecting changes in the spectral information spatially throughout a single flame and over various equivalency ratios, this preliminary analysis of a laminar calibration flame has opened the door to the use of IFTS cameras for combustion diagnostics. Spatially resolved spectral information provides a rudimentary view of the location of key chemicals in the flame as well as important information useful in the development of an initial radiative transfer model. Using this information and the exploitation of flame symmetry have made it possible to retrieve temperature and concentration estimates in the flame. Spectrally estimated temperatures agree with those obtained by OH-absorption measurement of a similar flame. Retrieved mixing fractions of H_2O and CO_2 are systematically too large as compared to equilibrium calculations. Further analysis is required to ascertain if this is due to path length and mixing layer effects., however a spectral model that does not assume symmetry through the flame is in development and should enable more accurate species mole fractions as well as a layered temperature estimate.

Appendix A. Long-wave IFTS measurements of laboratory scale laminar flame

1.1 Abstract

A point-and-shoot, passive remote sensing technology is highly desired to accurately monitor the combustion efficiency of petrochemical flares. A Phase II DOE-funded SBIR effort is being led by Spectral Sciences, Inc. to develop the methodologies needed to enable remote combustion efficiency measurements via spectral remote sensing. Part of this effort entails standing up a laboratory-scale flare measurement laboratory to develop and validate combustion efficiency measurements. This paper presents an overview and summarizes current progress of the Air Force Institute of Technology's contribution to this multi-organization, two-year effort. As a first step, a Telops Hyper-Cam longwave infrared (750–$1300\,\mathrm{cm}^{-1}$ or 7.7–$13.3\ \mu\mathrm{m}$) imaging Fourier-transform spectrometer is used to examine a laminar, calibration flame produced by a Hencken burner. Ethylene and propane were combusted under several different fuel/air mixing ratios. For each event, 300 hyperspectral datacubes were collected on a $172\,(W) \times 200\,(H)$ pixel window at a $1.5\,\mathrm{cm}^{-1}$ spectral resolution. Each pixel had approximately a $1.5 \times 1.5\,\mathrm{mm}^2$ instantaneous field-of-view. Structured emission is evident throughout the combustion region with several lines arising from H_2O; other lines have not yet been assigned. These first known imaging Fourier-transform spectrometer measurements of a laminar Hencken-burner flame are presented along with some preliminary analysis. While the laminar flame appears stationary to the eye, significant flame flicker at a fundamental frequency of $17\,\mathrm{Hz}$ was observed in the longwave infrared, and this is expected to complicate spectral interpretation for species concentrations and temperature retrieval. Changes to the

fuel-air ratio produced sizable changes in spectral intensity. Combustion spectra of ethylene and propane corresponding to ideal fuel-air ratio were nearly identical.

1.2 Introduction

Petrochemical and other industries routinely use open-air flares to dispose of combustible waste gases. Under ideal conditions, all carbon and hydrogen in the waste gas are converted to CO_2 and H_2O. When the combustion is incomplete, particulate material and Highly-Reactive Volatile Organic Compounds (HR-VOCs) can be released into the atmosphere posing environmental and health risks. Many flaring operations are not instrumented with *in situ* diagnostics to monitor Combustion Efficiency[1] (CE), and the cost of retro-fitting flares with instrumentation is high. Point-sampling methods can be highly accurate, but such methods are impractical to implement on a large scale. Spectral remote sensing techniques have the potential to fill an important role in real-time monitoring of CE. Active techniques such as Open-Path Fourier-Transform Infra-Red (OP-FTIR) spectrometry measurements and standard Fourier-Transform Spectrometry (FTS) have been successfully used to study flares throughout the years [1, 2]. However, for CE determination, OP-FTIR methods require the flare exhaust gases to be precisely positioned between the instrument and a retro-reflector so that plume transmission can be estimated. As the prevailing winds change direction, the plume can quickly wander out of the fixed Line-of-sight (LOS) transmission measurement. Both industry and environmental agencies desire a "point-and-shoot" system which can rapidly and accurately assess CE. While in principle spectral remote sensing methods are capable of solving this problem, to date, a passive, easily deployed remote sensor and an associated analysis

---

[1] Here, combustion efficiency is defined as the ratio of carbon converted to CO_2 relative to the total amount of carbon in the fuel.

methodology have not been developed which enable simple, robust quantification of flare CE.

Only recently has Imaging Fourier-Transform Spectrometry (IFTS) become commercially available [18, 31, 32, 33], and it could potentially be used to remotely estimate flare CE. We've previously demonstrated the capability of IFTS to accurately quantify smokestack effluents [4]. The dynamic nature of flare plumes makes the problem more challenging than the smokestack problem, but the principles of data collection and analysis are similar. With an appropriate field-of-view, IFTS can capture both the plume—regardless of the wind direction—and background in the same data set. The arbitrary pixels corresponding to post-flame combustion gases can be dynamically selected as the plume wanders across the Field-of-View (FOV). The simultaneous collection of background data simplifies both data capture and interpretation. Passive IFTS captures photons emitted via spontaneous emission from thermally excited gases in the flare plume, so positioning of a source (or retro-reflector) is unnecessary. Since IFTS is a passive technique, it may not have the sensitivity of an active measurement. However, the ability to selectively average arbitrary flare plume pixels can help improve sensitivity without the downside of including non-flare sources.

Spectral Sciences, Inc. is leading a project in conjunction with The University of Utah and The Air Force Institute of Technology (AFIT) to develop a system for the real-time remote monitoring of CE and HR-VOCs in industrial flares. Spectral Sciences, Inc. are developing the radiative transfer models necessary to simulate flare plume spectra in the infrared. The University of Utah team will apply their state-of-the-art Computational Fluid Dynamic (CFD) and chemical reaction models to predict flare flow-field parameters including temperature, gas density, and species concentrations throughout the entire flare plume. AFIT is standing up a laboratory-

scale flare testing facility and will provide temporally- and spatially-resolved infrared spectra which will be used to validate and improve the reactive-flow CFD and radiative transfer models.

This paper presents AFITs initial efforts in establishing the flare measurement facility. The first step in this effort is generating an ideal combustion source which can be operated at various combustion efficiencies. This will be used to calibrate and test both *in situ* and spectral remote sensing CE measurements. We report on IFTS measurements made by our Telops LWIR Hyper-Cam IFTS against a laminar flame source burning either ethylene or propane at several fuel to air ratios.

1.3 Experimental

1.3.1 Equipment description

The Telops Hyper-Cam [18, 31, 32, 33] is based on a traditional Michelson interferometer with a Mercury Cadmium Telluride (HgCdTe) FPA. The full 320×256 pixel set of the array can be sub-windowed to enable faster acquisition rates at the expense of spatial resolution. The spectral range covers $750\text{--}1300 cm^{-1}, (7.7\text{--}13.3\mu\text{m})$, and the spectral resolution can be arbitrarily selected within $0.25\text{--}150\,\text{cm}^{-1}$. Each pixel has a $0.35\,\text{mrad}$ instantaneous field-of-view (IFOV). An interferometric data cube is stack of images collected at fixed Optical Path Differences (OPDs). Fourier-transformation of each pixel's interferogram produces a raw hyperspectral image. Two on-board, aperture-filling blackbodies enable accurate spectro-radiometric calibration using a standard two-point, linear correction[19].

1.3.2 Laboratory measurements

The flames analyzed in this paper are an ethylene/air mixture and propane/air mixture (both at several ratios as described below) generated by a Hencken burner.

51
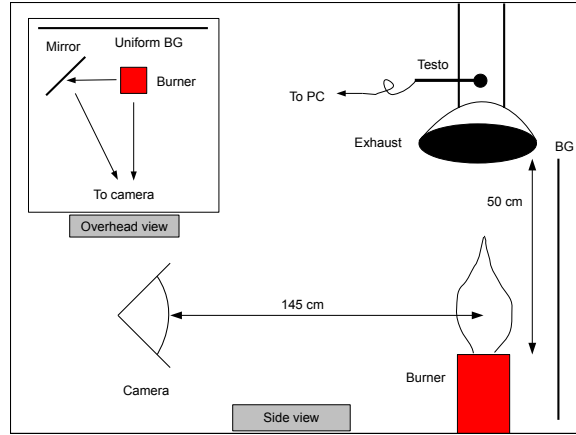
Figure 15. Rendering of experimental setup. The mirror was in an angled position to the left of the burner. This allowed for a complete reflected side view without interrupting the view of the burner and the uniform background. An exhaust pipe was positioned directly above the burner. The Testo measuring input was placed just within the entrance of the exhaust housing.

This burner generates a stable, laminar, nearly adiabatic flame ideal for developing and testing combustion diagnostics [14]. It has an inner burning surface with exit dimensions of $24.5 \times 24.5 \, \text{mm}^2$ and an outer housing of $38 \times 38 \, \text{mm}^2$. The Telops Hyper-Cam was set approximately 145 cm from the center of the burner flame. The burner was placed directly beneath an exhaust vent and in front of a sheet of Thor Labs BkF24 flat black aluminum in an attempt to provide a uniform background to the scene. The ratio of fuel to air being burned was adjustable and three separate burn types were recorded for both ethylene and propane. The ratios and room conditions during data capture are summarize in Table 2.

The Hyper-Cam was windowed to $172 \, (W) \times 200 \, (H)$ pixels just above the burner. This allowed for a complete view of the flame and the reflected image while still granting access to pixels which could be sampled as background. Camera integration time was set at 120 μs, which enabled good signal-to-noise without saturation. A spectral resolution of $1.5 \, \text{cm}^{-1}$ was used in acquisition to ensure suitably resolved spectra with datacubes of manageable size for transfer and processing. Radiometric calibration to radiance with units $\text{W}/(\text{cm}^2 \cdot \text{sr} \cdot \text{cm}^{-1})$ was accomplished using two

52

Table 2. Several ratios of fuel to air were chosen for analysis to represent various types of burn conditions. The flow of air and fuel were metered in Standard Liters Per Minute (SLPM) with a MKS-ALTA digital mass flow controller and set prior to data capture. Ambient data was recorded at the camera ($\sim 1.5\,m$ from the flame) using a Kestrel 4500 NV Weather Meter.

Fuel / Air Ratio	Flame Type	Fuel	Room Temp [ºC]	Humidity [%]	Pressure [hPa]
1.13/14.16 = 0.080	Ideal (blue)	Ethylene	25.7	50	977.9
0.66/14.15 = 0.046	Oxygen rich	Ethylene	25.7	49.7	977.9
1.63/8.65 = 0.188	Fuel rich (yellow)	Ethylene	25.9	49.3	977.8
0.57/11.15 = 0.051	Ideal (blue)	Propane	24.2	49.7	977.4
0.58/13.15 = 0.044	Oxygen rich	Propane	23.9	50.5	977.3
0.75/8.65 = 0.087	Fuel rich (yellow)	Propane	24.8	48.8	977.3

on-board blackbodies set at 60°C and 30°C. Calibration occurred both prior to and after each set of flame measurements.

A $200 \times 200\,\mathrm{mm}^2$ Thor Labs ME8S-G01 Protected Aluminum IR reflective mirror was placed angled and offset to the left of the burner. This mirror provided an additional view of the flame to allow for this analysis and future development of a 3D flame characterization model. It has an average reflectivity exceeding $96\,\%$ from $800\,\mathrm{nm}$ to $20\,\mu$ m. Unfortunately, the distance between the flame and background was insufficient to prevent thermal heating of the background. As a result, a slight temperature gradient which increased throughout the measurement was apparent in the data. The background of the mirror image was also of a Thor Labs flat black aluminum sheet. This sheet was much farther from the flame and did not suffer this problem. For this reason, the preliminary analysis presented in this paper will be of the flame as imaged in the mirror. A schematic detailing the experimental set-up is provided in Figure 15.

A Kestrel 4500 NV Weather Meter was used to intermittently capture ambient temperature, pressure, and humidity at the camera. The laboratory climate control system was turned off during most of the experimentation to minimize any influence

53

of drafts on the flame, but this did cause the temperature in the lab to fluctuate throughout the capture session. During the Ethylene burning session an average ambient temperature of 25.7°C, pressure of 977.9 hPa, and humidity of 46.0 % were found. Averages of 24.3°C, 977.3 hPa, and 46.3 % were calculated for the Propane measurements.

A Testo 350 Gas Analyzer was mounted just within the exhaust duct to allow for sampling of exhaust gases. This is an industry-standard instrument for *in situ* flue gas analysis. The system measures temperature, pressure, flow rate, and concentrations of carbon dioxide, carbon monoxide, molecular oxygen, nitrogen oxides, sulfur dioxide, and total hydrocarbons. Data from this analyzer was remotely recorded throughout the experiment for truth data confirmation of any spectral results found during analysis; however, the instrument was not properly calibrated and the Testo data recorded during this experiment was not used. The discrepancy will be corrected for future experiments and truth data will simultaneously be captured during spectral imaging.

1.4 Results and Discussion

1.4.1 Raw spectrum and flicker frequency

To the eye, the Hencken burner produces a stationary, laminar blue flame when burning a stoichiometric mixture of fuel and air. Surprisingly, the flame appeared considerably more dynamic in the long-wave infrared. Figure 16 presents an overview of the raw data collected from the IFTS. In the left panel, a non-uniformity corrected broadband image from an ethylene flame interferogram cube is presented. The interferogram corresponding to the highlighted pixel is presented in the top-right panel. Clearly evident is a sizable, low-frequency intensity oscillation on which the high-frequency interferogram rides on. A Butterworth low- and high-pass filter have been

54

applied to the measured interferogram and are presented for comparison. The raw and filtered interferograms are presented on the same scale with only a linear shift applied for convenient viewing. The amplitude of the low-frequency "flicker" is large compared to the high-frequency components which encode the infrared spectrum.

Examination of the sequential DC-level imagery (i.e., a movie) within an interferogram cube reveals a harmonic pulsation in the flame responsible for the flicker observed in the single-pixel interferogram. Since the camera frame rate is known, the frequency of this oscillation can be determined using the same Fourier transformation which produces the infrared spectrum. The bottom panel presents the magnitude of the interferogram's FFT. Both a wavenumber axis and frequency axis are provided[2] However, since the focal plane array records the broadband DC level, the frequency of plume fluctuations can also be determined if it falls outside the detector bandwidth. Examination of the out-of-band spectrum reveals that the flame's flicker frequency is approximately 17 Hz. This flicker is fairly well-defined with a spread of only a few Hz. The inset figure in the bottom panel shows a temporal sequence of DC images of images. The effect of this pulsation is evident on the flame structure. The cause of this flicker is currently under investigation.

The effect of this scintillation noise has not yet been assessed but is expected to be important in properly interpreting the spectrum [34]. We plan to apply the quantile interferogram processing method[35] to see if the effects of scintillation noise can be minimized.

1.4.2 Flame imagery and spectrum

This work examines the combustion behavior in the flame by comparing the ratio of several prominent spectral features at several locations throughout the flame. Vari-

---

[2] The IFTS camera is triggered to capture an image every fifth zero crossing of the HeNe metrology signal. Thus, this system samples on a fixed OPD grid and not on a fixed clock cycle. Small fluctuations in mirror velocity will introduce subtle errors in frequency analysis.
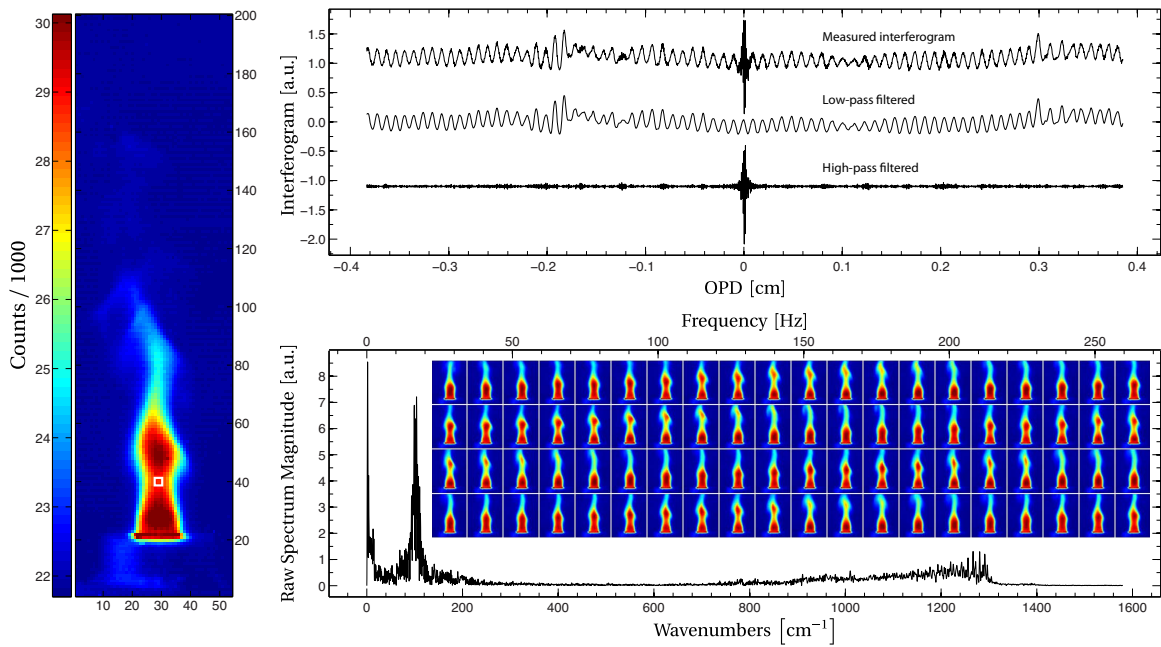
Figure 16. *Left panel:* **False-color DC image of the flame from the mirror image indicating the single-pixel featured in the other two panels.** *Top-right panel:* **Interferogram for a flame pixel approximately one flame diameter above the Hencken burner exit. Low- and high-pass filtered interferograms are also shown.** *Bottom-right panel*: **Raw spectrum corresponding to the single-pixel interferogram shown from $0\,\mathrm{cm^{-1}}$ to $1580\,\mathrm{cm^{-1}}$ (the Nyquist frequency). A cropped image sequence of the DC imagery illustrates the low-frequency ($\sim 17\,\mathrm{Hz}$) flame flicker. (Color available on line.)**

ations in the fuel-to-air ratio (FAR) were chosen because they each gave a distinct flame characteristic.
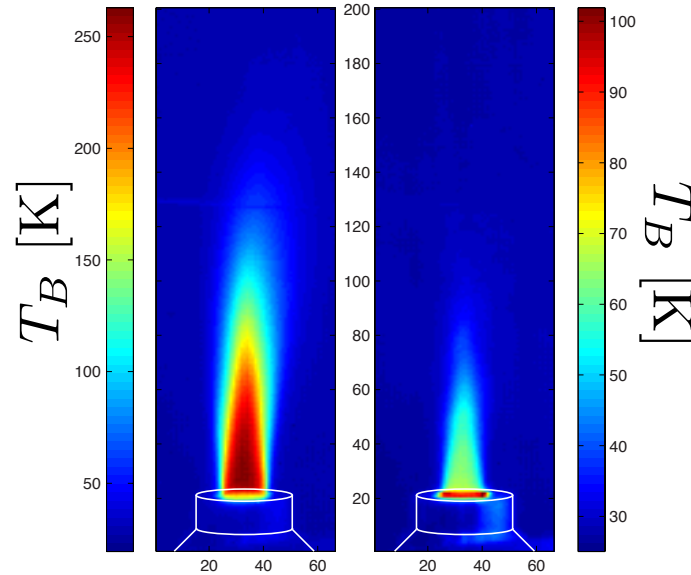
Figure 17. *Left panel:* False-color brightness temperature map at $\tilde{\nu} = 1267\,\mathrm{cm}^{-1}$ corresponding to a H_2O emission feature. *Right panel:* Brightness temperature map of the time-averaged radiance at $\tilde{\nu} = 1048\,\mathrm{cm}^{-1}$ representing variations in continuum emission. Both images correspond to ethylene combustion at the ideal fuel-to-air ratio. White lines indicate the approximate location of the Hencken burner.

When fuel-rich (large FAR), the Hencken burner produced a yellow flame typical of most refinery flairs. The fuel-lean (small FAR) condition produced a flame that was nearly transparent and light blue in color. The nearly stochiometric FAR produced a bright blue flame. The goal of choosing three diverse fuel mixtures was to achieve a variation in the spectrum of the exhaust that could be characterized and associated with the change.

A brightness temperature spatial map is provided in Figure 17 at two distinct frequencies. The left panel shown in Figure 17 represents a brightness temperature plot of the time-averaged radiance at $\tilde{\nu} = 1267$ cm^{-1} which corresponds to a water emission feature. Recall that this image was collected via the mirror reflection of the

57

Hencken burner (see Figure 15). The choice to use the reflected imagery of the flame was made due to complications with the background used. The flat black aluminum immediately behind the Hencken burner was positioned too closely to the flame and allowed a background thermal gradient to develop during the measurement. To provide uniformity in future work, a more robust background specifically designed for this experimental setup will be used. The right panel shown in Figure 17 shows a brightness temperature plot of the time-averaged radiance at $\tilde{\nu} = 1013$ cm^{-1}. There is no selective emission at this wavenumber so this plot represents variations in continuum emission. This continuum emission radiance could be caused by soot or other particulates in the air. The horizontal line present just above row 120 corresponds to the seam where the two 6" square mirrors are joined together. The flame imagery indicates a slight lean to the right side of the mirror, representing a bend of the flame away from the camera. The Kestrel weather meter did not register any wind velocity around the flame. It is not known if this is due to a small wind current in the room or a flow gradient at the exit of the Hencken Burner. The top panel of Figure 18 shows the spectrum of all three fuel-to-air ratios for ethylene combustion at pixel $(R, C) = (80, 35)$. (See Figure 17 for reference.)

Each spectrum is characterized by strong selective radiation, and many of the emission lines appear to be from hot H_2O. Transitions from carbon dioxide have not been identified. The CO_2 ν_2 fundamental bending mode at 667 cm^{-1} falls just outside of the HgCdTe FPA's detector response. The ν_1 symmetric stretching mode at 1388 cm^{-1} is not infrared active as it produces no change to the molecular dipole moment. It can be seen that the flame at all three FARs exhibit the same emission features with the major difference being that of absolute intensity. This may be caused by both temperature and concentration differences. The FAR was varied to induce a change in the CE of the Hencken burner with an expectation of observing

58
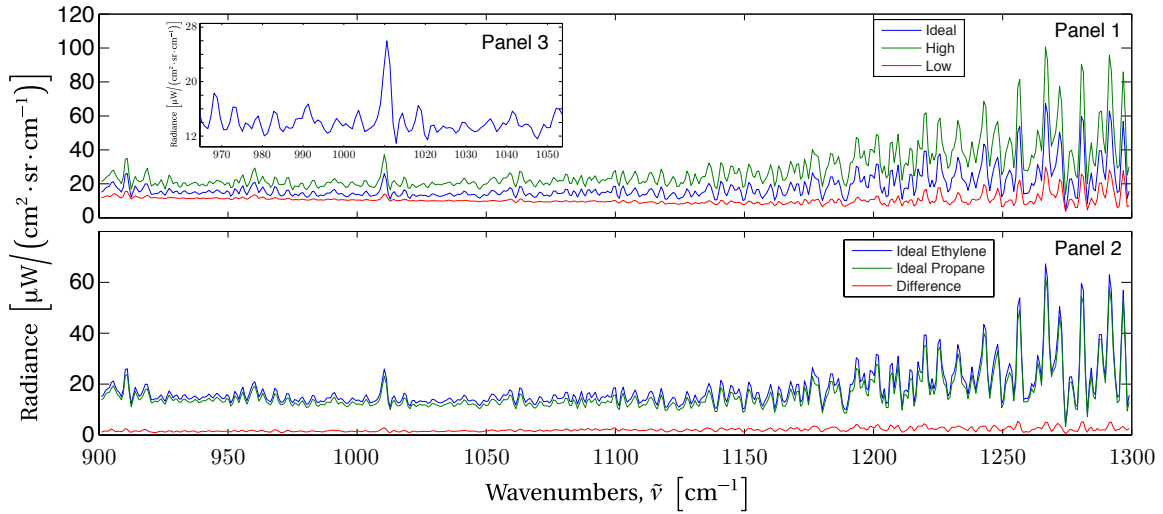
Figure 18. *Panel 1*: **Spectra of an ethylene combustion flame corresponding to three different fuel-to-air ratios. Spectrum taken from pixel** $(R, C) = (80, 35)$. *Panel 2*: **Comparison of ethylene and propane flame spectra at pixel** $(R, C) = (80, 35)$, **each combusting under ideal fuel-to-air ratios. The difference between the two spectra is also presented.** *Panel 3*: **Close look at the ideal ethylene spectrum around the emission line** $\tilde{\nu} = 1011 \, \text{cm}^{-1}$.

quantifiable changes in the measured spectra. However, estimation of CE will not be possible until the spectrum is fully assigned.

The bottom panel in Figure 18 compares the spectra of ethylene and propane combustion at the ideal (stochiometric) FAR at the same pixel $(R, C) = (80, 35)$. The difference between the two spectra is also provided and demonstrates their similarity in the LWIR. We anticipate incorporation of our MWIR Hyper-Cam in these flame measurements will enable identification and eventual quantification of additional species (e.g., CO and NO_x). Quantification of carbon-containing molecules is critical to the estimation of combustion efficiency. Truth measurements of combustion efficiency will be measured using the Testo 350 flue gas analyzer. Unfortunately, full calibration of this flue gas instrument was not completed in time to provide baseline data in this work.

59

1.4.3 Spectral model development

A radiative transfer spectral model is currently being developed to properly interpret the Hencken burner flame spectra. The model is currently simple and assumes a single, homogeneous layer in local thermodynamic equilibrium. Under these conditions, the Line-by-Line Radiative Transfer Model (LBLRTM[23]) is used in conjunction with the high-temperature (HITEMP[21]) extension of the HITRAN [22] spectral line database to generate flame spectra.
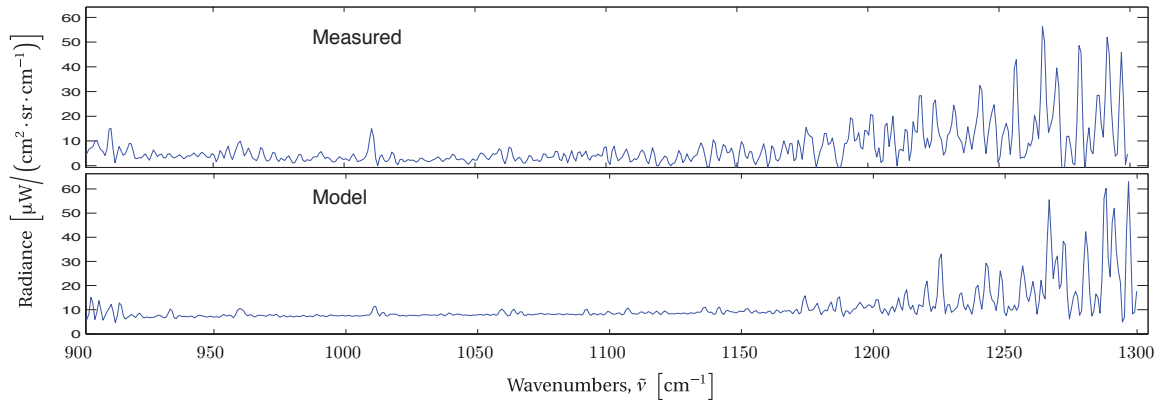
Figure 19. *Top Panel*: **Spectrum of data gathered at pixel** $(R, C) = (80, 35)$ **of the ideal ethylene flame.** *Bottom Panel*: **Simple model of the emission spectrum produced using HITRAN database.**

Figure 19 shows a comparison between the flame data taken at pixel $(R, C) = (80, 35)$ and the model simulation. For a better image of the selective emission comparison between both graphs, a baseline curve has been subtracted from both spectra. This model currently only uses the high temperature H_2O lines and assumes a flame temperature of $1273.15\,\mathrm{K}$, H_2O volume mixing fraction of 20%, and a plume path length of $6\,\mathrm{cm}$. Future measurements will be made at higher spectral resolution to ensure proper identification of additional gases (e.g., unburned or partially-oxidized organic compounds) present in the flame. If significant interferant gases are present,

60

retrieval of temperature and water concentration may need to be performed in spectral windows containing only H_2O lines. Most anticipated interferant gases will not be incorporated into the spectral model as the HITEMP database only contains lines for H_2O, CO_2, CO, NO, and OH. This is due to the difficulties in performing precise gas-phase spectroscopic measurements at high temperatures as well as challenges in making theoretical predictions of line positions and intensities for complicated organic molecules.

1.5 Conclusion

The first spatially-resolved, LWIR spectral measurements of a Hencken burner laminar flame have been presented. Propane and ethylene were observed under fuel-lean, ideal, and fuel-rich combustion conditions. While the flame appears stable, a strong flicker with an approximate frequency of $17\,\mathrm{Hz}$ was observed in the infrared. The effect of this harmonic noise source on the spectrum will need to be characterized before quantitative spectral analysis can be performed. Qualitative assessment of the spectra reveals substantial line emission from water. While expected to be present in the flame, CO_2 was not spectrally identified in the emission spectra. The fundamental ν_1 mode at $667\,\mathrm{cm}^{-1}$ of carbon dioxide falls below the FPA response and weaker CO_2 combination bands have not yet been identified. Variations in the fuel-to-air ratio produced significant changes to the measured spectrum with overall intensity increasing with FAR. At the ideal FAR, both ethylene and propane produced similar emission spectra.

Future measurements will incorporate both LWIR and MWIR IFTS and focus on the region above the combustion flame. This will enable identification of a wider range of species and should enable non-contact estimation of combustion efficiency. This preliminary analysis of a laminar calibration flame is the first of many key steps

toward the ultimate goal of real-time, continuous monitoring of full-scale industrial flares. The joint effort for the real-time remote monitoring of CE and HR-VOCs in flares is a large scale project and this work will eventually support the testing and validation of the CFD and radiative transfer models being developed for flares.

More generally, these preliminary measurements begin to demonstrate the potential of IFTS as a useful non-intrusive combustion diagnostic. With the development of an appropriate radiative transfer model and exploitation of flame symmetry, it may be possible to retrieve temperature and concentration profiles throughout the entire combustion flame. However, substantial work is needed to bring this diagnostic to fruition.

Appendix B. Effects of Flicker Frequency on Spectral line-shape in the long-wave IR

This appendix expands on the discussion in Chapter III regarding a model created to understand the effects the flame pulsation has on the spectral line shape generated from an averaged interferogram. Included are full details of the model as well as the model results performed in the Long-Wave IR region covered in Appendix A.

2.1   Model Details

As mentioned in Chapter III, each interferogram gathered showed a sizable ($\approx 20\%$ of full intensity, see Figure 4) harmonic fluctuation in measured D.C. level intensity. The high frequency spectral information desired rides on this D.C. level. To improve the signal-to-noise ratio, many interferograms of the same scene are usually averaged. Each of the 500 data cubes measured for this work have a random starting phase to the D.C. fluctuation and averaging them removes this fluctuation creating a constant D.C. level. As Equation 2 suggests, the desired intensity $I_{AC}(x)$ is intimately connected to the D.C. level intensity $I_{DC}(x)$. Average together many values of $I_{i,j}(x)$ visually changes the I_{DC} value. If I_{AC} is also effected the spectral radiance model (Equation 3) would not produce accurate results. To test this a model was produce interferograms that replicate this situation.

First, a spectrum of the wavenumber band of interest was generated using a constant temperature of 1750 K. This was done using LBLRTM [23] and spectral lines from the HITRAN [22] database. This spectrum then was converted to an interferogram, representing one not influenced by an average over several interferograms with a random phase flicker. Secondly, 1000 spectra with a 17 Hz flicker and 200 K amplitude ranging from 1650 K and 1850 K were created, also using LBLRTM and HITRAN. Each of these 1000 interferograms was assigned a random starting phase

63

similar to the actual data, and were averaged together. This created a single interferogram with a constant D.C. level intensity simmilar to a scene at 1750 K. Any difference between this and the first interferogram should be a result of the averaging process. Both interferograms were converted back into spectra and compared (Figure 5). The results of the comparison show that there is no significant difference between a spectrum generated from one single interferogram at a mean temperature of 1750 K and a spectrum generated from the average of the 1000 interferograms with a 17 Hz flicker with a 200 K amplitude ranging from 1650 K and 1850 K.

2.2 Long-Wave model results
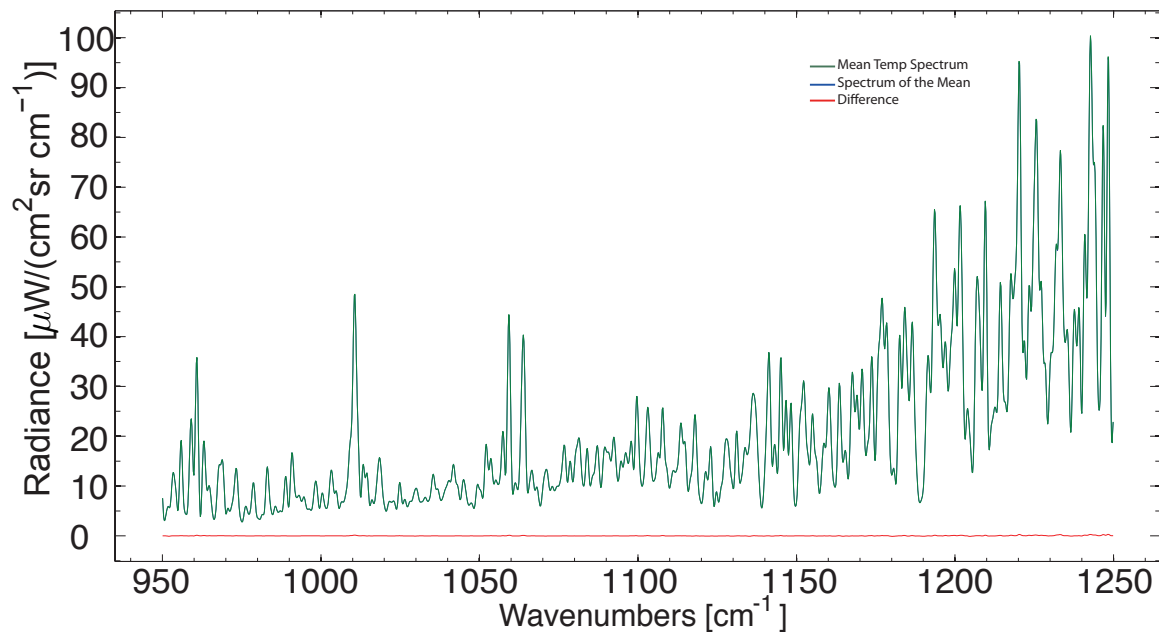
Figure 20. Simulation of the effect of averaging over 1000 interferograms each with a random starting phase for a harmonic 17Hz, 200 K fluctuation in signal level. Performed over the Long-Wave IR region of 950 to 1250 cm^{-1}

The paper presented in Appendix A mentions the concern felt regarding the effects the flicker may have on the spectral line-shape but this model had not been created

at the time of the papers completion. The results of the LW are then presented here. In the data set gatherd by the LW camera, the Michelson mirror scanned as a velocity almost three times slower then the data sets measured by the MW camera. This difference in scan velocity makes it neccicary to redo the model for the LW dataset. As Figure 20 shows though, there is no measurable difference between the two spectra and it can be concluded that averaging the interferograms has no effect on the spectral line-shape.

Appendix C. Additional details on IFTS calibration

The recored intensity $I_{i,j}(x)$ at the IFTS detector consists of modulation from the scanning Michelson $\cos(2\pi\tilde{\nu}x)$, the instrument response $G(\tilde{\nu})$ and the scene spectrum $L_{i,j}(\tilde{\nu})$.

$$I_{i,j}(x) = \frac{1}{2}\int_0^\infty [1 + \cos(2\pi\tilde{\nu}x)]G(\tilde{\nu})L_{i,j}(\tilde{\nu})\mathrm{d}\tilde{\nu} = I_{DC} + I_{AC}(x). \tag{8}$$

This combined effect results in an interferogram like the one pictured in Figure 4. For a static scene, the interferogram $I_{i,j}(x)$ can be expressed as a constant I_{DC} — the broadband spectrally-integrated signal — and a modulated component $I_{AC}(x)$. To estimate temperature and species concentrations the developed model must be fit to the spectral information $L_{i,j}(\tilde{\nu})$ only. The first step then is to isolate $I_{AC}(x)$ by a simple subtraction $I_{AC}(x) = I_{DC} - I_{i,j}(x)$. The results of this are pictured in Figure 21.
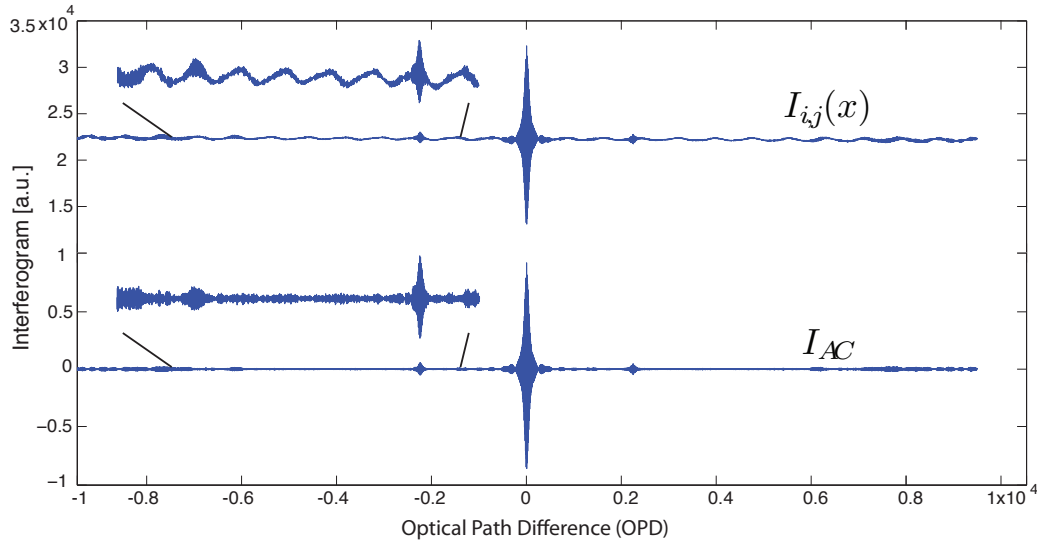

Figure 21. Top: Raw interferogram of the $\Phi = 1.25$ flame at pixel (i, j) = (30 mm, 0 mm). Inset images is an enhanced section of the interferogram to emphasize the effects of the DC intensity. Bottom: Interferogram including only the I_{AC} signal. Inset image is again an enhanced section of the interferogram.

66

Clearly visible is a drop in the intensity values from an oscillation point around 2.25×10^4 to 0. This is a result of removing the primary DC level offset. Also, as discussed previously, the intensity changes associated with the flame flicker are removed as they are also DC level signal changes. Now that the I_{AC} signal is isolated it can be converted to a spectrum $Y_{i,j}(\nu)$ via a Fourier-transformation, displayed in Figure 22. This spectrum though still includes the effects of the instrument response and any internal noise the instrument may have. To remove these effects the spectrum must be calibrated using a standard two-point calibration [19]. This requires interferogram measurements from two blackbodies at known temperatures. Calibration blackbodies emit a radiance curve that has values well defined by Plancks blackbody radiance $B(\tilde{\nu}, T)$ at any given temperature T and wavenumber $\tilde{\nu}$.

$$B(\tilde{\nu}, T) = \frac{2hc^2\tilde{\nu}^3}{e^{\frac{hc}{kT}\tilde{\nu}} - 1}. \tag{9}$$

Here c is the speed of light, h is Plancks constant and k is Boltzmann constant. Due to the instrument response and any internal noise the measured radiance will differ from the ideal blackbody radiance. A unique gain G and offset O must be calculated for each point in the spectrum and at each pixel to quantify the unique effects of the camera.

The gain of the camera is defined as

$$G_{i,j}(\nu) = \frac{Y1 - Y2}{B1 - B2} \tag{10}$$

where Y1 and Y2 are the raw spectrum associated with the hotter and colder blackbodies respectfully. B1 and B2 are the calibration radiances from the ideal Planckian curve at the given temperatures of blackbodies 1 and 2. The offset value

is given by

$$O_{i,j}(\nu) = \frac{(Y2 * B1) - (Y1 * B2)}{Y1 - Y2} \tag{11}$$

Once the gain and offset are calculated they can be applied to the uncalibrated spectrum $Y_{i,j}(\nu)$ very simply to achieve a calibrated radiance spectrum $L_{i,j}(\nu)$.

$$L_{i,j}(\nu) = \frac{Y_{i,j}(\nu)}{G_{i,j}(\nu)} - O_{i,j}(\nu) \tag{12}$$

Figure 22 shows a comparison of a raw spectrum $Y_{i,j}(\nu)$ and a calibrated spectrum $L_{i,j}(\nu)$.
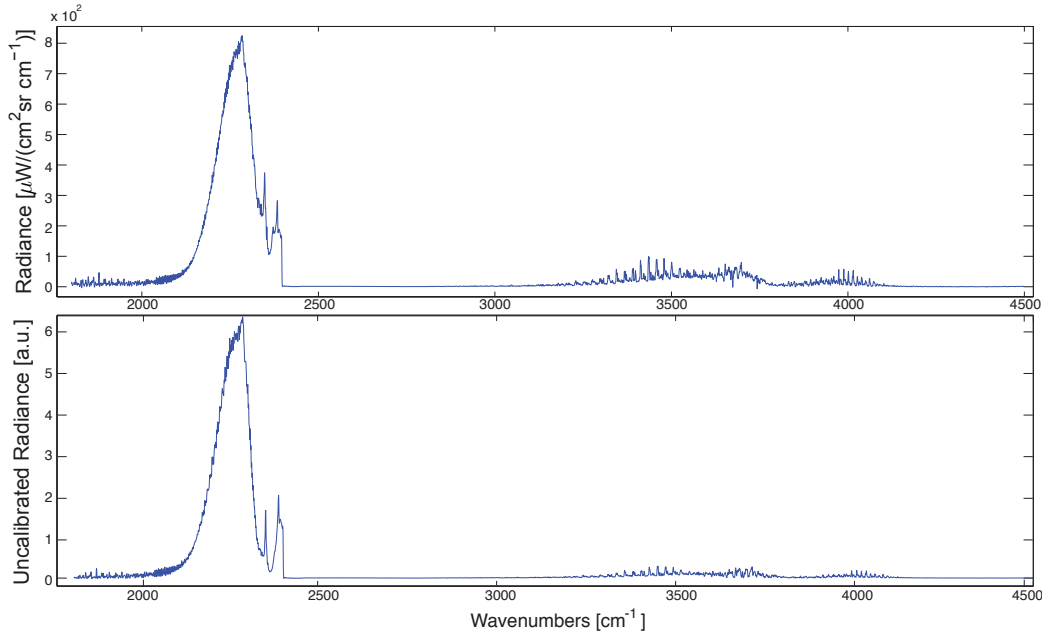
Figure 22. Comparison between an uncalibrated spectrum from the $\Phi = 1.25$ flame at pixel (i, j) = (30 mm, 0 mm) and a calibrated spectrum also from the $\Phi = 1.25$ flame at pixel (i, j) = (30 mm, 0 mm)

Appendix D. Additional details on the spectral model

This appendix provides additional details on the spectral model used in Chapters III and IV through an explanation of each term in the equation. Following this will be several visual examples of the effects temperature species concentration changes have on the spectral model. Here the equation for the spectral model radiance $L(\tilde{\nu})$ is restated:

$$L(\tilde{\nu}) = \tau(\tilde{\nu})\varepsilon(\tilde{\nu}, \xi_\kappa)B(\tilde{\nu}, T) \tag{13}$$

The first variable is the atmospheric transmittance $\tau(\tilde{\nu})$. This variable models the fraction of light that passes successfully through the thickness of air between the flame and the instrument. The values then range from 1 - representing 100% transmittance of light - to 0 or total absorption of light. Transmittance value depends on wavenumber, species concentration and the thickness of the atmosphere the light must pass through. The dependance on length is strait forward, farther distances gives the light a greater chance to be absorbed. The wavenumber dependance however is a bit more complicated. Most absorption occurs from the H_2O and CO_2 present in air and is dependent on the concentration and absorption cross section $\sigma(\tilde{\nu})$ of these two chemicals. For this model $\tau(\tilde{\nu})$ is calculated using LBLRTM [23] and the HITRAN [22] database. HITRAN supplies the location of spectral features associates with atmospheric H_2O and CO_2 along with values for $\sigma(\tilde{\nu})$ and LBLRTM uses that information along with a user imputed values for path length and mole fraction of H_2O and CO_2 to generate a transmittance profile for a desired spectral band. Figure 23 shows two transmittance profiles for the spectral band used in this work. The first has an atmospheric path length of 3 m and the second has a path length of 3 km. The effects of additional atmosphere are very noticeable especially around the areas of ~ 2350 cm^{-1} and ~ 4350 cm^{-1}

69
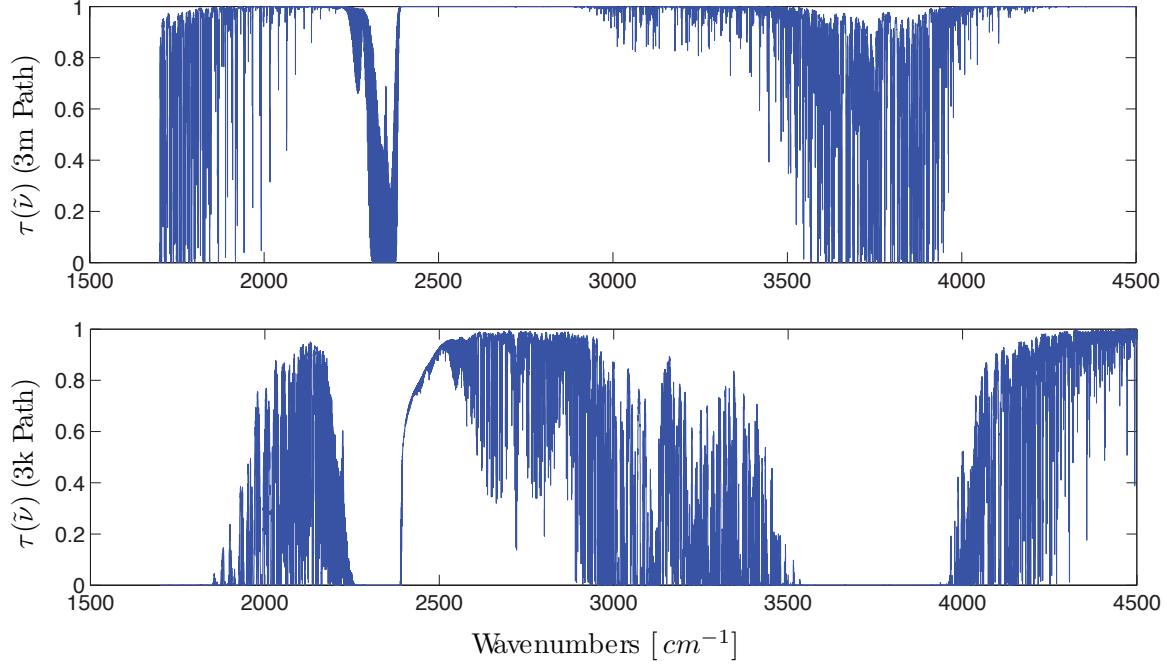
Figure 23. LBLRTM generated atmospheric transmittance profile for H_2O and CO_2. Top panel represents transmittance through 3 meters of air. Bottom panel represents transmittance through 3 kilometers of air.

The second variable is $\varepsilon(\tilde{\nu}, \xi_\kappa)$ or the emissivity of the gasses in the hot flame. This represents the probability that a given chemical will emit a photon at a given wavelength. This can be expressed as

$$\varepsilon(\tilde{\nu}, \xi_k) = 1 - \exp\left(-Nl \sum_k \xi_k \sigma_k(\tilde{\nu}, T)\right) \tag{14}$$

where $N = P/(k_B T)$ is the total gas number density, l is the path length through the flame and σ_k is the Boltzmann-weighted absorption cross-section for species k and ξ_k the gas mole fractions. This expression is also 1 - $\tau(\tilde{\nu})$ where $\tau(\tilde{\nu})$ is now the transmissivity of the flame rather than the atmosphere. This is possible based off the assumption that the flame is optically thin. Weighting σ_k becomes important here because the elevated temperature of the gasses pushes gas population into higher

70

energy levels following the Boltzmann distribution. Weighting the cross section by the Boltzmann distribution assigns a probability to each cross section based on the probability that a photon of a given energy will be absorbed for a given population distribution. In short, more molecules in the correct energy state the more likely the photon will be absorbed and the hotter the gas the more populated the higher energy levels will be. The total gas number density is calculated from the assumption of an even 1 atm pressure value and similar to the atmospheric transmittance, path length l of the flame is a user impute value. The temperature of the flame and the the gas mole fractions ξ_k however are the desired values and they are left as adjustable variables in the model fit. Figure 24 shows the estimated emissivity of the flame over a set of various conditions. First is the emissivity at a temperature of 1750 K and with equal parts H_2O and CO_2 at a concentration of $0.13x10^6$ ppmv. The second graph changes the temperature to 500 K and keeps the chemical concentrations the same. The third graph keeps a temperature of 1750 K and changes the chemical concentration of H_2O to $0.065x10^6$ ppmv, half that of CO_2. The final graph again keeps the temperature at 1750 K and this time adjusts the CO_2 value to $0.065x10^6$ ppmv, half that of H_2O.

Figure 24 shows the effects of temperature on emissivity, clearly seen between the first and second graphs. The emissivity features of H_2O and CO_2 shorten and spread out as the hot gasses populate a broader amount of energy states. Also the emissivity feature with the highest peak for each chemical changes, shifting outward towards the edges of the feature. In contrast, comparing graph 1 to 2 and 3 shows the effects concentration changes has on the emissivity. The location of the features remains constant but their relative heights lower with lower concentration, a simple result of less gas to emit photons.

The final variable is the Plancks blackbody radiance $B(\tilde{\nu})$ for a given temperature
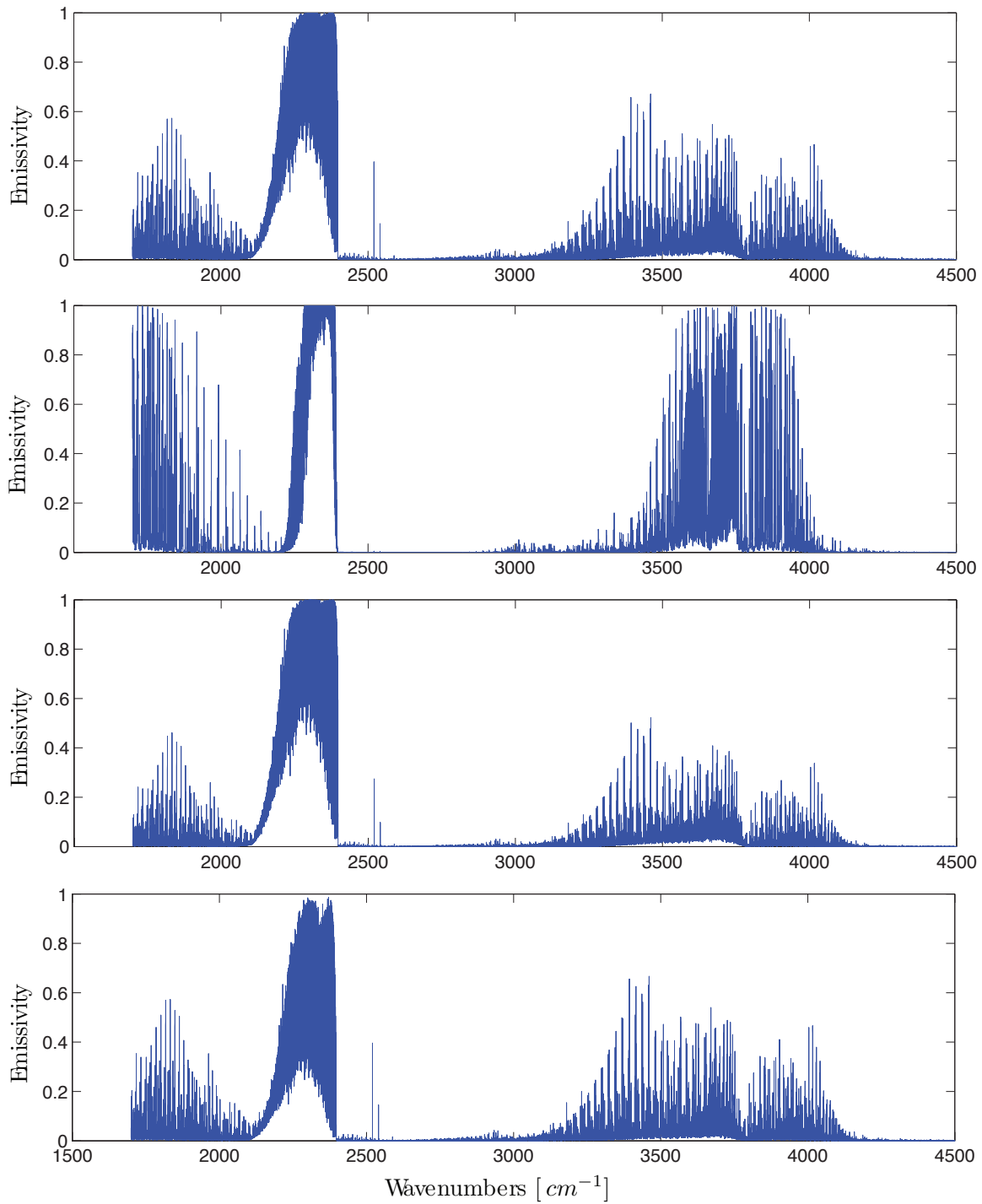
Figure 24. Estimated flame emissivity over a set of various conditions. (1) Emissivity at a temperature of 1750 K, equal parts H_2O and CO_2 at a concentration of 0.13×10^6 ppmv. (2) Emissivity at temperature of 500 K, concentrations the same. (3) Emissivity at temperature of 1750 K, chemical concentration of H_2O to 0.065×10^6 ppmv, half that of CO_2. (4) Emissivity at a temperature of 1750 K chemical concentration of CO_2 to 0.065×10^6 ppmv, half that of H_2O.

72

T. This variable adjusts the total radiance levels according to the Plancian curve associates with the estimated temperature T. Putting it all together the model spectral radiance is fit to the measured radiance using a Nelder-Mead direct search followed by Levenberg-Marquardt gradient-based error minimization. The adjustable variables are the flame temperature and the chemical concentrations. When the residuals of the model fit are minimized and show no systematic errors there is reason to believe that the temperature and chemical concentrations estimated by the model are the temperature and chemical concentrations present in the flame.

Bibliography

[1] T.R. Blackwood. An evaluation of flare combustion efficiency using open-path fourier transform infrared technology. *Journal of the Air and Waste Management Association*, 50:1714–1722, 2000.

[2] J. Joda Wormhoudt. Infrared methods for gaseou smeasurements. *Optical Engineering*, 7, 1985.

[3] T. Wootton J. Moncrieff A. K. Chambers, M. Strosher and P. McCready. Dial measurements of fugitive emissions from natural gas plants and the comparison with emission factor estimates. *Proc. 15th International Emission Inventory Conference*, 2006.

[4] Kevin C. Gross, Kenneth C. Bradley, and Glen P. Perram. Remote identification and quantification of industrial smokestack effluents via imaging fourier-transform spectroscopy. *Environmental Science and Technology*, 44(24):9390 – 9397, 2010.

[5] Jacob L. Harley and Kevin C. Gross. Remote quantification of smokestack effluent mass flow rates using imaging fourier transform spectrometry. volume 8018, page 801813. SPIE, 2011.

[6] Terrence R. Meyer, Sukesh Roy, Thomas N. Anderson, Joseph D. Miller, Viswanath R. Katta, Robert P. Lucht, and James R. Gord. Measurements of oh mole fraction and temperature up to 20 khz by using a diode-laser-based uv absorption sensor. *Appl. Opt.*, 44(31):6729–6740, Nov 2005.

[7] M. McDaniel. Flare efficiency study. *EPA Contract*, 68-02-3541-6, July 1968.

[8] T. S. Cheng, J. A. Wehrmeyer, and R. W. Pitz. Laser raman diagnostics in subsonic and supersonic turbulent jet diffusion flames. *NASA Contractor Report*, 1991.

[9] R.S. Barlow and C.D. Carter. Raman/rayleigh/lif measurements of nitric oxide formation in turbulent hydrogen jet flames. *Combustion and Flame*, 97(3–4):261 – 280, 1994.

[10] A.C. Eckbreth. *Laser Diagnostics for Combustion Temperature and Species*. Combustion Science and Technology Book Series. Gordon and Breach Publishers, 1996.

[11] David Blunck, Sumit Basu, Yuan Zheng, Viswanath Katta, and Jay Gore. Simultaneous water vapor concentration and temperature measurements in unsteady hydrogen flames. *Proceedings of the Combustion Institute*, 32(2):2527 – 2534, 2009.

74

[12] U. Platt and J. Stutz. *Differential Optical Absorption Spectroscopy: Principles And Applications.* Physics of Earth And Space Environments. Springer, 2007.

[13] Pierre Tremblay, Simon Savary, Matthias Rolland, Andre Villemaire, Martin Chamberland, Vincent Farley, Louis Brault, Jean Giroux, Jean-Luc Allard, Eric Dupuis, and Tiarles Padia. Standoff gas identification and quantification from turbulent stack plumes with an imaging fourier-transform spectrometer. volume 7673, page 76730H. SPIE, 2010.

[14] P. J. Lakusta. Laser-induced fluorescence and performance analysis of the ultra-compact combustor. *Thesis, Air Force Institute of Technology*, 2003.

[15] M. S. Woodridge, P. V. Torek, M.T. Donovan, D. L. Hall, T. A. Miller, T. R. Palmer, and C. R. Schrock. An experimental investigation of gas-phase combustion synthesis of sio2 nanoparticals using a multi-element diffusion flame burner. *Combustion and Flame*, 131:98–109, 2002.

[16] K. Hencken. Research technologies. inc. *Pleasanton, CA*.

[17] Kevin C. Gross, Pierre Tremblay, Kenneth C. Bradley, Martin Chamberland, Vincent Farley, and Glen P. Perram. Instrument calibration and lineshape modeling for ultraspectral imagery measurements of industrial smokestack emissions. volume 7695, page 769516. SPIE, 2010.

[18] Farley V., Vallieres A., Chamberland M., Villemaire A., and Legault J. F. Performance of the first, a longwave infrared hyperspectral imaging sensor. Number 6398, 63980T-1. SPIE, 2006.

[19] Henry E. Revercomb, H. Buijs, Hugh B. Howell, D. D. LaPorte, William L. Smith, and L. A. Sromovsky. Radiometric calibration of ir fourier transform spectrometers: solution to a problem with the high-resolution interferometer sounder. *Appl. Opt.*, 27(15):3210–3218, Aug 1988.

[20] P. R. Griffiths and J. A. de Haseth. *Fourier Transform Infrared Spectrometry.* 2007.

[21] L.S. Rothman, I.E. Gordon, R.J. Barber, H. Dothe, R.R. Gamache, A. Goldman, V.I. Perevalov, S.A. Tashkun, and J. Tennyson. Hitemp, the high-temperature molecular spectroscopic database. *Journal of Quantitative Spectroscopy and Radiative Transfer*, 111(15):2139 – 2150, 2010. ¡ce:title¿XVIth Symposium on High Resolution Molecular Spectroscopy (HighRus-2009)¡/ce:title¿ ¡xocs:fullname¿XVIth Symposium on High Resolution Molecular Spectroscopy¡/xocs:fullname¿.

[22] L.S. Rothman, I.E. Gordon, A. Barbe, D.Chris Benner, P.F. Bernath, M. Birk, V. Boudon, L.R. Brown, A. Campargue, J.-P. Champion, K. Chance, L.H. Coudert, V. Dana, V.M. Devi, S. Fally, J.-M. Flaud, R.R. Gamache, A. Goldman,

D. Jacquemart, I. Kleiner, N. Lacome, W.J. Lafferty, J.-Y. Mandin, S.T. Massie, S.N. Mikhailenko, C.E. Miller, N. Moazzen-Ahmadi, O.V. Naumenko, A.V. Nikitin, J. Orphal, V.I. Perevalov, A. Perrin, A. Predoi-Cross, C.P. Rinsland, M. Rotger, M. Šimečková, M.A.H. Smith, K. Sung, S.A. Tashkun, J. Tennyson, R.A. Toth, A.C. Vandaele, and J. Vander Auwera. The hitran 2008 molecular spectroscopic database. *Journal of Quantitative Spectroscopy and Radiative Transfer*, 110(9–10):533 – 572, 2009. ¡ce:title¿HITRAN¡/ce:title¿.

[23] S.A. Clough, M.W. Shephard, E.J. Mlawer, J.S. Delamere, M.J. Iacono, K. Cady-Pereira, S. Boukabara, and P.D. Brown. Atmospheric radiative transfer modeling: a summary of the aer codes. *Journal of Quantitative Spectroscopy and Radiative Transfer*, 91(2):233 – 244, 2005.

[24] Kostiuk L. W. and Cheng R. K. The coupling of conical wrinkled laminar flames with gravity. *Combustion and Flame*, 103:27–40, 1995.

[25] W. M. G. Malalasekera, H. K. Versteeg, and K. Gilchrist. A review of research and an experimental study on the pulsation of buoyant diffusion flames and pool fires. *Fire and Materials*, 20(6):261–271, 1996.

[26] Shepherd I. G., Cheng R. K., and Day M. S. The dynamics of flame flicker in conical premixed flames: An experimental and numerical study. Colloquium: 4. Laminar Flames. Lawrence Berkeley National Laboratory.

[27] S. Gordon and B. J. McBride. *Computer program for calculation of complex chemical equilibrium compositions and applications*. 1996.

[28] S. Roy, P. J. Kinnius, R. P. Lucht, and J. R. Gord. Temperature measurements in reacting flows by time-resolved femtosecond coherent anti-stokes raman scattering (fs-cars) spectroscopy. *Optics Communications*, 281:319–325, 2008.

[29] K. E.; Hancock, R. D.; Bertagnolli and R. P. Lucht. Nitrogen and hydrogen cars temperature measurements in a hydrogen/air flame using a near-adiabatic flat-flame burner. *Combustion and Flame*, 109:323–331, 1997.

[30] Kaushik Biswas, Yuan Zheng, Chul Han Kim, and Jay Gore. Stochastic time series analysis of pulsating buoyant pool fires. *Proceedings of the Combustion Institute*, 31(2):2581 – 2588, 2007.

[31] V. Farley, C. Belzile, M. Chamberland, J.-F. Legault, and K. R. Schwantes. Development and testing of a hyperspectral imaging instrument for field spectroscopy. volume 5564, pages 29–36. SPIE, 2004.

[32] M. Chamberland, V. Farley, P. Tremblay, and J.-F. Legault. Performance model of imaging fts as a standoff chemical agent detection tool. volume 5268, pages 240–251. SPIE, 2004.

[33] Martin Chamberland, Vincent Farley, Alexandre Vallieres, Andre Villemaire, Louis Belhumeur, Jean Giroux, and Jean-Francois Legault. High-performance field-portable imaging radiometric spectrometer technology for hyperspectral imaging applications. volume 5994, page 59940N. SPIE, 2005.

[34] D. D. Klug and E. Whalley. Effects of source noise in fourier-transform spectroscopy. *Journal of the Optical Society of America*, 64(7):1019–1020, 1974.

[35] P. Tremblay, K. C. Gross, V. Farley, M. Chamberland, and A. Villemaire. Understanding and overcoming scene-change artifacts in imaging fourier-transform spectroscopy of turbulent jet engine exhaust. volume 7457, page 74570F. SPIE, Aug 2009.

REPORT DOCUMENTATION PAGE

Form Approved
OMB No. 0704–0188

1. REPORT DATE *(DD–MM–YYYY)*	2. REPORT TYPE	3. DATES COVERED *(From — To)*
14–06–2012	Master's Thesis	1 Sep 2010 - 14 June 2012

4. TITLE AND SUBTITLE

Application of an Imaging Fourier-Transform Spectrometer for the Means of Combustion Diagnostics

5a. CONTRACT NUMBER

5b. GRANT NUMBER

DESC0003373

5c. PROGRAM ELEMENT NUMBER

6. AUTHOR(S)

Michael R. Rhoby

5d. PROJECT NUMBER

12P724

5e. TASK NUMBER

5f. WORK UNIT NUMBER

7. PERFORMING ORGANIZATION NAME(S) AND ADDRESS(ES)

Air Force Institute of Technology
Graduate School of Engineering and Management (AFIT/EN)
2950 Hobson Way
WPAFB OH 45433-7765

8. PERFORMING ORGANIZATION REPORT NUMBER

AFIT/OSE/ENP/12 − J02

9. SPONSORING / MONITORING AGENCY NAME(S) AND ADDRESS(ES)

Spectral Sciences, Inc. (Dr. Raphael Panfili)
4 Fourth Avenue
Burlington, MA 01803-3304
1-781-273-4700 rpanfili@spectral.com

10. SPONSOR/MONITOR'S ACRONYM(S)

SSI

11. SPONSOR/MONITOR'S REPORT NUMBER(S)

12. DISTRIBUTION / AVAILABILITY STATEMENT

APPROVED FOR PUBLIC RELEASE; DISTRIBUTION UNLIMITED.

13. SUPPLEMENTARY NOTES

14. ABSTRACT

A passive remote sensing technique for accurately monitoring the combustion efficiency of petrochemical flares is greatly desired. A Phase II DOE-funded SBIR lead by Spectral Sciences, Inc. is underway to develop such a method. This paper presents an overview of the progress of AFIT's contribution. A Telops Hyper-Cam Mid-wave infrared imaging Fourier-transform spectrometer is used to examine a flame produced by a Hencken burner. Ethylene fuel was burned at four different equivalency ratios $\Phi = 0.80, 0.91, 1.0$ and 1.25. Presented is qualitative spectrally-resolved visualization of a Hencken burner flame and the spatial distribution of combustion by-products. The flame spectra were characterized by structured emissions from CO_2, H_2O and CO. A single-layer model is developed to estimate the temperature and H_2O and CO_2 concentrations using spectrally-resolved flame emissions between $3100 \text{ cm}^{-1} \leq \nu \leq 3500 \text{ cm}^{-1}$. At the flame center 10 mm above the burner, temperature was estimated as $T = 2172 \pm 28$ K, this compares favorably with recently reported OH-absorption measurements ($T = 2226 \pm 112$ K) and equilibrium calculations ($T = 2302$ K). H_2O and CO_2 mole fractions at the same height of 10 mm were measured to be $13.7 \pm 0.6\%$ and $15.5 \pm 0.8\%$, respectively.

15. SUBJECT TERMS

Imaging Fourier-transform spectrometer, Combustion, Laminar flame, Flue gas analysis

16. SECURITY CLASSIFICATION OF:			17. LIMITATION OF ABSTRACT	18. NUMBER OF PAGES	19a. NAME OF RESPONSIBLE PERSON
a. REPORT	b. ABSTRACT	c. THIS PAGE			Dr. Kevin C. Gross, AFIT/ENP
U	U	U	UU	76	19b. TELEPHONE NUMBER *(include area code)* (937)255-3636 x4558;kevin.gross@afit.edu

Standard Form 298 (Rev. 8–98)
Prescribed by ANSI Std. Z39.18